SIAM J. APPL. MATH.
Vol. 73, No. 2, pp. 853–881

CONDITIONS FOR TRANSIENT VIREMIA IN DETERMINISTIC IN-HOST MODELS: VIRAL BLIPS NEED NO EXOGENOUS TRIGGER*

WENJING ZHANG†, LINDI M. WAHL†, AND PEI YU‡

Abstract. This paper presents an analytical study of the phenomenon of recurrent infection, that is, transient episodes of high viral reproduction, separated by long periods of relative quiescence, which are observed in many persistent infections; the "viral blips" observed during chronic infection with human immunodeficiency virus (HIV) are a well-known example. Although in-host models which incorporate forcing functions or stochastic elements have been proposed to generate viral blips, simple deterministic models also exhibit this phenomenon. Analyzing a 4-dimensional HIV antioxidant-therapy model which exhibits viral blips, we show that an increasing, saturating infectivity function may contribute to the recurrent behavior of the model. We then propose four conditions for the existence of viral blips in a deterministic in-host infection model. We use these conditions to derive the simplest (2- and 3-dimensional) infection model which produces viral blips, and we determine the complete parameter range for the 3-dimensional model in which blips are possible, using stability analysis. We also use these conditions to demonstrate that low-dimensional in-host models with linear or constant infectivity functions cannot generate viral blips. Further, we find that a 5-dimensional immunological model satisfies the conditions and exhibits recurrent infection even with constant infectivity; thus, an increasing, saturating infectivity is not necessary if the model is sufficiently complex.

Key words. recurrent infection, HIV viral blips, bifurcation theory, dynamical system

AMS subject classifications. 92D30, 37L10, 37N25

DOI. 10.1137/120884535

1. Introduction.

Viruses are infectious intracellular parasites: they can reproduce only inside the living cells of host organisms and must spread from host to host for continued existence. Animal viruses tend to exhibit either an acute or persistent mode of host infection to ensure this continuity [40]. An acute viral infection is characterized by a relatively short period of symptoms and resolution within days or weeks. It usually triggers the host immune response to clear the infection, and a memory response can then prevent the same virus from infecting the same host. Pathogens such as influenza virus and rhinovirus typically cause acute viral infections. In contrast, persistent infections [3] establish long-lasting infections in which the virus is not fully eliminated but remains in infected cells. Persistent infections involve both silent and productive infection stages without rapid killing or excessive damage to infected cells. Latent infection is a type of persistent infection.

In latent infection, no clinical signs nor detectable infectious cells can be observed during the silent or quiescent stage of low-level viral replication. However, the virus has not been completely cleared, and recurrent episodes of rapid viral production and release can periodically punctuate relatively long periods in the silent stage. These episodes of recurrent infection are a clinical phenomenon observed in many latent

*Received by the editors July 13, 2012; accepted for publication (in revised form) January 15, 2013; published electronically April 10, 2013. This work was supported by the Natural Sciences and Engineering Research Council of Canada (NSERC).
http://www.siam.org/journals/siap/73-2/88453.html
†Applied Mathematics, University of Western Ontario, London, Ontario, N6A 5B7 Canada (wzhan88@uwo.ca, lwahl@uwo.ca).
‡Corresponding author. Applied Mathematics, University of Western Ontario, London, Ontario, N6A 5B7 Canada (pyu@uwo.ca).

infections [41]. Recurrent infection can also occur in the context of drug treatment for persistent infections. Human immunodeficiency virus (HIV), for instance, can be suppressed by highly active antiretroviral therapy (HAART) to below the limit of detection for months or years [5, 8]; nonetheless supersensitive assays can still detect low levels of viremia during this stage [8, 31, 30]. Moreover, these long periods of relative quiescence are typically interrupted by unexplained intermittent episodes of viremia above the detectable limit, termed viral blips [35, 34]. Although these blips have been the focus of much recent research [12, 17, 14, 6], their etiology is still not well understood [17, 34].

To date, many possible explanations for viral blips during HIV infection have been explored mathematically. An early model of the long-term pathogenesis of HIV [11] incorporates the activation of T cells in response to antigen, as suggested earlier by [9]. In [11], both HIV and non-HIV antigen exposure are considered in a coupled deterministic-stochastic model. The probability of antigenic exposure evolves continuously in time, and Poisson-distributed exposure events are generated, by simulation, at the appropriate probabilities. This approach captures a number of features of long-term HIV dynamics, including episodic "bursts" of residual viral replication. Further work [10] considers the number of distinct antigens which activate the $CD4^+$ T cell pool as a random variable, coupled to an ordinary differential equation (ODE) model. Stochastic changes to this number drive fluctuation in the basic reproductive number and viral load. This model is also able to capture the episodic burst-like nature of residual HIV viral replication during long-term infection.

More recent models are based on the recurrent activation of latently infected lymphocytes, a class of T cells introduced in immunological models by Perelson et al. [32] and Rong, Feng, and Perelson [33], in order to explain the slower second-phase decay of plasma viremia. By introducing antigen concentrations as an explicit variable, Jones and Perelson [23] developed a system of ODEs which exhibits viral blips. The model describes programmed proliferation and contraction of the $CD8^+$ T cell population and exhibits low viral loads under HAART as expected. Opportunistic or concurrent infection, modeled as an initial concentration of antigen, activates the immune system and is shown by numerical simulation to elicit a transient viral blip. The same authors further showed that occasional intercurrent infections can generate viral blips by the activation of target cells or latently infected cells, predicting a power law relationship between blip amplitude and viral load [24].

In further work, by considering the asymmetric division of latently infected cells, Rong and Perelson [34] developed a 4-dimensional ODE model based on the basic model of latent cell activation [32]. This new model not only generated viral blips but also maintained a stable latent reservoir in patients on HAART. In this model, latently infected cells can divide to produce latently infected daughter cells, or differentiate into activated, productively infected cells, depending on antigen concentrations. In a further 5-dimensional ODE model [35], these two types of daughter cells were distinguished as dependent variables, and a contraction phase was added to the activated daughter cells. Numerical simulation showed that both cases gave rise to viral blips and a stable latent reservoir, which were generated from the activated and the latently infected daughter cells, respectively. In both papers [34, 35], the antigenic stimulation of latently infected cells was modeled as an "on-off" forcing function, and viral blips were initiated during brief pulses in which this activation function was "on."

Most recently, a stochastic model developed by Conway and Coombs [6] presented another possible treatment of latent cell activation. In this model [6], the authors derive the probability generating function for a multitype branching process describing

the populations of productively and latently infected cells and free virus. A numerical approach is then used to estimate the probability distribution for viral load, which is then used to predict blip amplitudes and frequencies; blip durations are studied by simulation. The authors are able to conclude that with effective drug treatment and perfect adherence to drug therapy, viral blips *cannot* be explained by stochastic activation of latently infected cells, and other factors such as transient secondary infections, or imperfect adherence, must be involved.

In order to elicit transient episodes of high viral replication, the models described above incorporate either transient immune stimulation, for example as a forcing function, or stochastic approaches. In contrast, recent studies have shown that simple deterministic systems can exhibit viral blips. Based on the close relation between recurrent infections and antibody (B-cell) immunodeficiency, Yao, Hertel, and Wahl [41] investigated a 5-dimensional ODE model which included antibody concentrations as an explicit variable and exhibited transient periods of high viral replication. By numerical simulation at specific, meaningful, parameter values, the authors explored factors affecting the interval between recurrent episodes and their severity. Later, an even simpler 4-dimensional antioxidant-therapy model [39] was explored for HIV and was similarly used to simulate viral blips with appropriate parameter values. These examples indicate that deterministic systems can produce blips as part of the natural, rich behavior of the nonlinear system. Although to date numerical simulation has been invaluable in describing and delineating the behavior of these models, there is as yet very little analytical work exploring the mathematical underpinnings of recurrent infection. It should be noted that data from clinical studies indicates that HIV viral blips appear to be random biological events, with varying magnitude, frequency, and duration. This suggests that stochastic models may be more realistic or appropriate for describing such phenomena. On the other hand, deterministic models are more tractable, and their analysis may reveal a global picture or key underlying characteristics of the system. Moreover, nonlinear deterministic systems can indeed exhibit varying amplitudes and frequencies of motion, particularly when the underlying parameters are functions of time. We shall return to a discussion of this point in the last section of the paper.

In this paper, we take advantage of dynamical systems theory to reinvestigate deterministic in-host infection models that exhibit viral blips. By examining the bifurcation behavior in parameter spaces "close" to the region where blips occur, we propose an understanding of the features of the dynamical system which underlie this complex model behavior. We then propose four conditions which, when satisfied, guarantee that an in-host infection model will exhibit long periods of quiescence, punctuated by brief periods of rapid replication—viral blips. Based on these conditions, we develop very simple 2- and 3-dimensional models that produce blips. Further, we apply stability criteria to determine parameter ranges which may yield blips. Most of the models discussed in this paper share a similar infectivity function, describing the rate at which new infected cells are created. In a final section, we examine a related 5-dimensional immunological model and demonstrate that viral blips are possible in this system even when infectivity is constant.

The rest of the paper is organized as follows. In section 2, the previously proposed 4-dimensional HIV antioxidant-therapy model is reinvestigated analytically. Based on the insights of our bifurcation analysis, conditions for generating viral blips are proposed. In section 3, we use these conditions to propose a simpler 3-dimensional in-host infection model, and parameter ranges which will exhibit blips in the simpler model are determined. In section 4, we develop a 2-dimensional model, characterized

by an increasing and saturating infectivity function, which can also generate viral blips. Finally, we demonstrate that a 5-dimensional immunological model [41] can exhibit viral blips with constant infectivity.

2. A 4-dimensional model which exhibits viral blips. In this section, we reconsider a 4-dimensional HIV antioxidant-supplementation therapy model which was developed and studied numerically in [39]. This model novelly introduced reactive oxygen species (ROS) and antioxidants to an in-host model of HIV infection. In uninfected individuals, ROS play a positive physiological role at moderate levels [16, 25, 7, 20, 18] but are harmful at high levels [39].

HIV infection may lead to chronic and acute inflammatory diseases, which may cause high levels of ROS [26] as well as lowered antioxidant levels; this phenomenon has been observed clinically and experimentally [26, 15, 22, 36, 38]. In addition, high levels of ROS may cause damage to $CD4^+$ T cells, impair the immune response to HIV [37], and exacerbate infected cell apoptosis, releasing more HIV virions. Thus, infected cells produce high levels of ROS, which in turn increase the viral production by infected cells. To control this cycle, antioxidant supplementation (vitamin therapy) has been suggested as a potential complement to HIV therapy [15, 13], with the aim of counteracting and reducing ROS concentrations [16].

The equations of the 4-dimensional model are described by [39]:

$$\begin{aligned} \dot{x} &= \lambda_x - d_x x - (1-\epsilon)\beta(r)xy, \\ \dot{y} &= (1-\epsilon)\beta(r)xy - d_y y, \\ \dot{r} &= \lambda_r + ky - mar - d_r r, \\ \dot{a} &= \lambda_a + \alpha - par - d_a a, \end{aligned} \tag{2.1}$$

where x, y, r, and a represent, respectively, the population densities of the uninfected $CD4^+$ T cells, infected $CD4^+$ T cells, ROS, and antioxidants. The constant λ_x denotes the production rate of $CD4^+$ T cells, and $d_x x$ is the death rate. Uninfected cells become infected at rate $(1-\epsilon)\beta(r)xy$, where ϵ is the effectiveness of drug therapy, and d_y is the per-capita death rate of infected $CD4^+$ T cells. ROS are generated naturally at rate λ_r, and by the infected cells at rate $k\,y$; the concentration of ROS decays at rate $d_r\,r$ and is eliminated by interaction with antioxidants at rate mar. Antioxidants are introduced into the model through natural dietary intake at a constant rate λ_a and through antioxidant supplementation at rate α, which is treated as a bifurcation parameter. Antioxidants are eliminated from the system by natural decay at rate $d_a a$ and by reacting with the ROS at rate par, where p is much smaller than m.

An important novel feature of this model is that the infectivity $\beta(r)$ is a positive, increasing, and saturating function of r (ROS),

$$\beta(r) = b_0 + \frac{r(b_{\max} - b_0)}{r + r_{\text{half}}}, \tag{2.2}$$

where b_0 represents the infection rate in the ROS-absent case, while $b_{\max}$ denotes the maximum infection rate, and r_{half} is the ROS concentration at half maximum. It is obvious that $\beta(r) > 0$, and it is also assumed that $0 < \epsilon < 1$. Therefore, all the parameters in (2.1) and (2.2) are positive. The experimental values used for studying model (2.1) are given in Table 2.1. Importantly, these parameters were chosen with careful reference to clinical studies, such that the predicted equilibrium densities are clinically reasonable. Also note that the densities of antioxidants and ROS are of order 10^{13} per μL, while cell densities are of the order 10^2 or 10^3 per μL.

TABLE 2.1
Parameter values used in model (2.1) [39].

Parameter	Value
λ_x	$60.76 \quad \text{cells}\,\mu\text{L}^{-1}\,\text{day}^{-1}$
d_x	$0.0570 \quad \text{day}^{-1}$
d_y	$1.0 \quad \text{day}^{-1}$
λ_a	$2.74 \times 10^{13} \quad \text{molecules}\,\mu\text{L}^{-1}\,\text{day}^{-1}$
d_a	$0.0347 \quad \text{day}^{-1}$
ε	$\frac{1}{3}$
b_0	$2.11 \times 10^{-4} \quad \text{cell}^{-1}\,\mu\text{L}\,\text{day}^{-1}$
$b_{\max}$	$0.00621 \quad \text{cell}^{-1}\,\mu\text{L}\,\text{day}^{-1}$
r_{half}	$3.57 \times 10^{13} \quad \text{molecules}\,\mu\text{L}^{-1}$
d_r	$1.66 \times 10^{7} \quad \text{day}^{-1}$
λ_r	$1.86 \times 10^{21} \quad \text{molecules}\,\mu\text{L}^{-1}\,\text{day}^{-1}$
k	$1.49 \times 10^{19} \quad \text{molecules}\,\text{cell}^{-1}\,\text{day}^{-1}$
m	$1.27 \times 10^{-6} \quad \text{molecule}^{-1}\,\mu\text{L}\,\text{day}^{-1}$
p	$5.04 \times 10^{-14} \quad \text{molecule}^{-1}\,\mu\text{L}\,\text{day}^{-1}$

In [39], this model was explored numerically to assess the potential of antioxidant therapy as a complement to HIV drug therapy. In that study, regions of oscillatory behavior, reminiscent of viral blips, were observed. In the following subsections we perform a thorough equilibrium and stability analysis of the model in order to shed further light on the factors underlying these rich behaviors.

2.1. Well-posedness of the solutions of system (2.1). By using the method of variation of constants, we can easily obtain the solutions of (2.1) to show that $x(t)>0$, $y(t)>0$, $r(t)>0$, $a(t)>0 \ \forall\, t>0$ if $x(0)>0$, $y(0)>0$, $r(0)>0, a(0)>0$. To consider the boundedness of the solutions, suppose in general we have the differential inequality $\dot{T} \le \lambda - dT$ (λ, $d>0$, $T(0)>0$). Then if $\dot{T} = \lambda - dT$, we have $\dot{T}+dT = \lambda$. Thus, $T(t) = T(0)e^{-\int_0^t d\,\mathrm{d}s} + \int_0^t \lambda\, e^{-\int_s^t d\,\mathrm{d}u}\mathrm{d}s = T(0)\, e^{-d\,t} + \frac{\lambda}{d}(1-e^{-d\,t})$, which implies that $\lim_{t\to+\infty} \sup T(t) = \frac{\lambda}{d}$. From the first equation of (2.1), we have $\dot{x} \le \lambda_x - d_x x$, which yields $\lim_{t\to+\infty} \sup x(t) = \frac{\lambda_x}{d_x}$. It is also easy to see from the first equation of (2.1) that $x(t) > 0\, \forall\, t > 0$. Then, by adding the first two equations of (2.1) we obtain $\frac{\mathrm{d}[x(t)+y(t)]}{\mathrm{d}t} = \lambda_x - d_x x - d_y y \le \lambda_x - \tilde{d}(x+y)$, where $\tilde{d} = \min(d_x, d_y)$. Hence, $\lim_{t\to+\infty} \sup(x(t)+y(t)) = \frac{\lambda_x}{\tilde{d}}$. Therefore, for any given $\varepsilon > 0$, there exists $t^* > 0$, such that $x + y \le \frac{\lambda_x}{\tilde{d}} + \varepsilon\, \forall\ t \ge t^*$. For the third equation of (2.1), we similarly have $\frac{\mathrm{d}r}{\mathrm{d}t} \le (\lambda_r + k\frac{\lambda_x}{\tilde{d}}) - d_r r$, which results in $\lim_{t\to+\infty} \sup r(t) = \frac{\lambda_r \tilde{d} + k\lambda_x}{d_r \tilde{d}}$. Finally, for the fourth equation of (2.1), we get $\frac{\mathrm{d}a}{\mathrm{d}t} \le (\lambda_a + \alpha) - d_a\, a$, and thus $\lim_{t\to+\infty} \sup a(t) = \frac{\lambda_a+\alpha}{d_a}$. We define

$$\Gamma = \left\{(x, y, a, r) \in R^4 \,\middle|\, 0 \le x \le \tfrac{\lambda_x}{d_x},\ 0 \le x+y \le \tfrac{\lambda_x}{\tilde{d}},\ 0 \le r \le \tfrac{\lambda_r + k\lambda_x/\tilde{d}}{d_r},\ 0 \le a \le \tfrac{\lambda_a+\alpha}{d_a}\right\}.$$

Clearly, Γ is a positively invariant set and attracts all nonnegative solutions of (2.1).

2.2. Equilibrium solutions of (2.1) and their stability. To find the equilibrium solutions of (2.1), simply setting $\dot{x} = \dot{y} = \dot{r} = \dot{a} = 0$ yields two solutions, the uninfected equilibrium solution E_0 and the infected equilibrium solution E_1, given, respectively, by

$$\mathrm{E}_0 : \ (x_{e0},\, y_{e0},\, r_{e0},\, a_{e0}) = \left(\frac{\lambda_x}{d_x},\, 0,\, r_{e0},\, \frac{\lambda_r - d_r\, r_{e0}}{m\, r_{e0}}\right), \tag{2.3}$$

where the r_{e0} is determined by the equation

$$F_0(r,\alpha) \equiv \alpha + \lambda_a + \frac{1}{m}\left(p\,d_r\,r - \frac{d_a\,\lambda_r}{r}\right) + \frac{d_a\,d_r - p\,\lambda_r}{m} = 0, \tag{2.4}$$

and

$$\begin{aligned} \mathrm{E}_1: \quad & \big(x_{e1}, y_{e1}, r_{e1}, a_{e1}\big), \quad x_{e1} = \frac{d_y}{(1-\epsilon)\,\beta_r(r_{e1})}, \\ & y_{e1} = \frac{\lambda_x - d_x\,x_{e1}}{(1-\epsilon)\beta_r(r_{e1})x_{e1}}, \quad a_{e1} = \frac{\lambda_a + \alpha}{d_a + p r_{e1}}, \end{aligned} \tag{2.5}$$

where r_{e1} is a function in the system parameters, particularly α (see the function F_1 in 2.8)). Both E_0 and E_1 are expressed in terms of r (r_{e0} or r_{e1}) for convenience.

We first consider the uninfected equilibrium E_0. The solution of r_{e0} is determined by (2.4), which is a quadratic equation in r. To simplify the analysis, we use r to express the parameter α since (2.4) is linear in α, and α is treated as a bifurcation parameter. Thus, solving $F_0(r,\alpha) = 0$ for α, we obtain

$$\alpha_0(r_{e0}) = -\lambda_a - \frac{1}{m}\left(p\,d_r\,r_{e0} - \frac{d_a\,\lambda_r}{r_{e0}}\right) - \frac{d_a\,d_r - p\,\lambda_r}{m}. \tag{2.6}$$

To find the stability of the equilibrium solution E_0, we first evaluate the Jacobian of system (2.1) at E_0 to get $J_0(r_{e0})$, where (2.6) has been used, and then we use $\det(\xi\,\mathrm{I} - J_0)$ to obtain the 4th-degree characteristic polynomial, given by $P_0(\xi, r_{e0}) = (\xi + d_x)\big[\xi^2 + (pr_{e0} + d_a + \frac{\lambda_r}{r_{e0}})\xi + (\frac{d_a\lambda_r}{r_{e0}} + pd_r r_{e0})\big](\xi + P_{0r})$, where

$$P_{0r} = d_y - \frac{(1-\epsilon)\lambda_x(b_0 r_{\mathrm{half}} + r_{e0} b_{\max})}{d_x(r_{e0} + r_{\mathrm{half}})}. \tag{2.7}$$

$P_0(\xi, r_{e0})$ contains three factors: the first is a linear polynomial of ξ, and the second is a quadratic polynomial of ξ, and both are stable polynomials (i.e., their roots (eigenvalues) have negative real part); and thus the stability of E_0 depends only on the third factor, a linear polynomial of ξ. Therefore, when $P_{0r} > 0$ ($P_{0r} < 0$), the equilibrium solution E_0 is asymptotically stable (unstable).

The graph for the equation $F_0(r,\alpha) = 0$ given in (2.4) is shown as the red line in Figure 2.1(a), which clearly shows a hyperbola. It is seen from this red line that the relation (2.4) also defines a single-valued function r in α if only the positive (biologically meaningful) value of r is considered (i.e., the positive branch of the red line in Figure 2.1(a)). More precisely, it can be shown that the biologically meaningful solution must be located on the first quadrant and above, including the top branch of the red line (see Figure 2.1(a)), since E_0 has the component $y_{e0} = 0$.

Next, consider the infected equilibrium solution E_1. The solution for r_{e1} can be similarly obtained by solving the equation

$$F_1(r,\alpha) = \lambda_r + \frac{k\lambda_x}{d_y} - \frac{kd_x(r + r_{\mathrm{half}})}{(1-\epsilon)(b_0 r_{\mathrm{half}} + b_{\max} r)} - \frac{mr(\lambda_a + \alpha)}{pr + d_a} - d_r r = 0, \tag{2.8}$$

which is again a linear function of α, and we can use r_{e1} to express α as

$$\begin{aligned} \alpha_1(r_{e1}) = & -\lambda_a + \frac{\lambda_r(pr_{e1} + d_a)}{mr_{e1}} + \frac{k\lambda_x(pr_{e1} + d_a)}{mr_{e1}d_y} \\ & - \frac{kd_x(r_{e1} + r_{\mathrm{half}})(pr_{e1} + d_a)}{mr_{e1}(1-\epsilon)(b_0 r_{\mathrm{half}} + b_{\max} r_{e1})} - \frac{(pr_{e1} + d_a)d_r}{m}. \end{aligned} \tag{2.9}$$

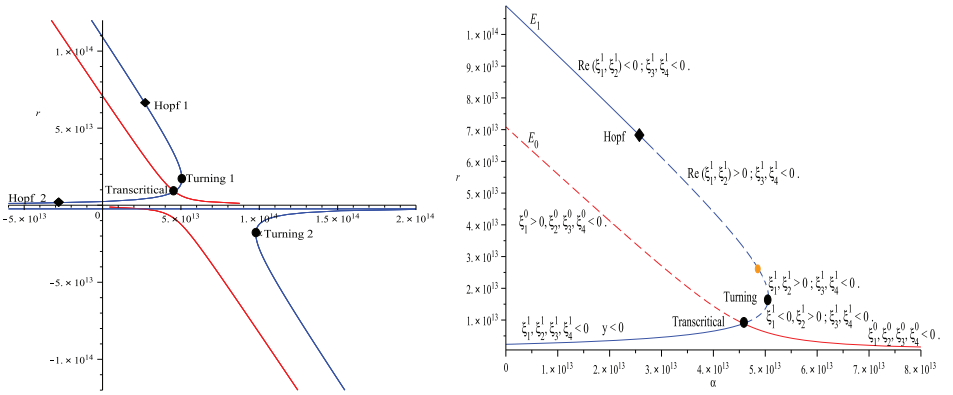

(a) (b)

FIG. 2.1. (a) *Complete bifurcation diagram for the* 4*-dimensional HIV antioxidant-therapy model* (2.1) *projected on the* r*-*α *plane, with the red and blue lines denoting* E_0 *and* E_1*, respectively.* (b) *Bifurcation diagram in* (a)*, restricted in the first quadrant, with the dotted and solid lines indicating unstable and stable, respectively.*

The graph of the equations $F_0(r,\alpha) = 0$ given in (2.4) and $F_1(r,\alpha) = 0$ given in (2.8) is shown in Figure 2.1(a). To find the stability of E_1, in a similar way, we evaluate the Jacobian of (2.1) at E_1 to obtain the 4th-degree characteristic polynomial, $P_1(\xi, r_{e1}) = \xi^4 + a_1(r_{e1})\xi^3 + a_2(r_{e1})\xi^2 + a_3(r_{e1})\xi + a_4(r_{e1})$, where the lengthy expressions for the coefficients $a_1(r_{e1})$, $a_2(r_{e1})$, $a_3(r_{e1})$, and $a_4(r_{e1})$ are omitted here for brevity.

2.3. Bifurcation analysis. To understand the conditions underlying oscillatory behavior and viral blips in this model, we now consider possible bifurcations which may occur from the equilibrium solutions E_0 and E_1.

2.3.1. Transcritical bifurcation. First, for the uninfected equilibrium E_0, it follows from $P_0(\xi, r_{e0})$ and (2.7) that in general E_0 is stable for $P_{0r} > 0$, and the only possible singularity occurs at the critical point, determined by $P_{0r} = 0$ (see (2.7)). At this point, one eigenvalue of the characteristic polynomial becomes zero (and the other three eigenvalues still have negative real part), leading to a static bifurcation, and E_0 becomes unstable. More precisely, when the parameter values in Table 2.1 are used, the two equilibrium solutions E_0 and E_1 intersect and exchange their stability at the point $(r_t, \alpha_t) \approx (8.89\times10^{12}, 4.58\times10^{13})$, indicating that a *transcritical bifurcation* occurs at this critical point (see Figure 2.1(b)). Here, the subscript "t" stands for transcritical bifurcation. The value of α_t is obtained by substituting r_t into either $\alpha_0(r_t)$ in (2.6) or $\alpha_1(r_t)$ in (2.9). In fact, $\alpha_0(r_t) = \alpha_1(r_t)$.

As discussed above, the biologically meaningful solutions should be above or on the uninfected equilibrium solution E_0 (the red line shown in Figure 2.1(b)), since solutions below the red line contain the component $y < 0$. It is obvious that there is no Hopf bifurcation from E_0. So, the uninfected equilibrium E_0 is asymptotically stable (unstable) when $r < r_t$ ($r > r_t$) or $\alpha > \alpha_t$ ($\alpha < \alpha_t$) (see Figure 2.1(b)).

It should also be noted from Figure 2.1(b) that besides a transcritical bifurcation point, E_1 has a *saddle-node* bifurcation which occurs at the so-called *turning point*. To determine this turning point, using (2.9) and $\frac{d\alpha_1(r)}{dr} = 0$ yields $(r_s, \alpha_s) \approx (1.72\times10^{13}, 5.06\times10^{13})$, where the subscript "s" denotes saddle-node bifurcation, and $\alpha_s = \alpha_1(r_s)$ by using (2.9). Note that this bifurcation does not change the sta-

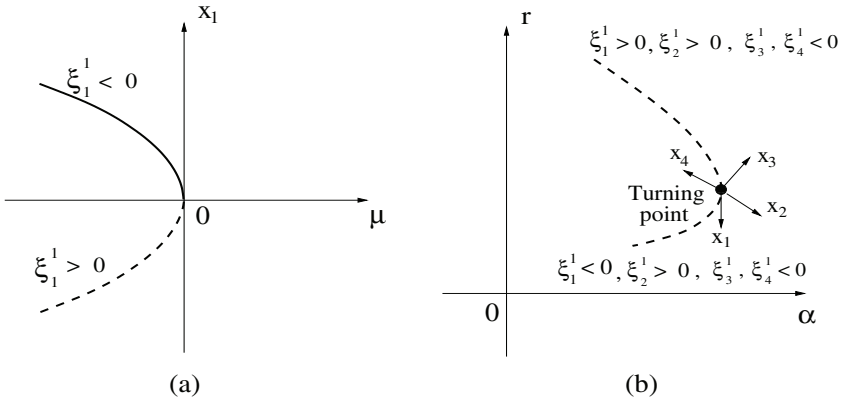

FIG. 2.2. *The saddle-node bifurcation on the center manifold with the dotted line indicating unstable and the solid line stable* (a) *in the transformed* x_1-μ *coordinates and* (b) *in the original coordinates.*

bility of E_1 since the characteristic polynomial $P_1(\xi, r_{e1})$ still has an eigenvalue with positive real part when r_{e1} (or α) is varied along E_1 to pass through the turning point (see Figure 2.1(b)).

The saddle-node bifurcation can be seen more clearly if we examine the local dynamics close to the turning point; this analysis will also be useful later for analyzing viral blips. At the turning point, the system contains a 1-dimensional center manifold (whose linear part is characterized by the eigenvalue $\xi_1^1 = 0$), a 1-dimensional unstable manifold (whose linear part is characterized by the eigenvalue $\xi_2^1 \approx 0.142$), and a 2-dimensional stable manifold (whose linear part is characterized by the eigenvalues $\xi_3^1 \approx -0.290$ and $\xi_4^1 \approx -1.26 \times 10^8$), as shown in Figure 2.2. It is noted that the eigenvalues ξ_2^1 and ξ_1^1, which are both positive at the saddle-node point, become a pair of complex conjugates with positive real part at the orange point above the saddle-node point (see Figure 2.1(b)), moving toward the Hopf point. So the submanifold that is the complement to the center manifold is still expelling until meeting the Hopf bifurcation point.

In order to find the differential equation described on the center manifold, we first apply the transformation $(x, y, r, a)^T = (x_{e1}, y_{e1}, r_{e1}, a_{e1})^T + T_s(x_1, x_2, x_3, x_4)^T$, where $(x_{e1}, y_{e1}, r_{e1}, a_{e1})$ is the infected equilibrium solution E_1, and T_s is a constant, nonsingular matrix. Under this transformation, the Jacobian of system (2.1) becomes the Jordan canonical form: $\Lambda_s \approx \text{diag}\,\{0,\ 0.142,\ -0.290,\ -1.26{\times}10^8\}$. Then, by using center manifold theory [19] on the transformed system of (2.1), we get the differential equation describing the dynamics of the system, restricted to the center manifold, $\dot{x}_1 \approx -2.66 \times 10^{-12}\mu - 1.93 \times 10^{-4} x_1^2$, for which the perturbation value of μ near the saddle-node point is roughly $\mu \approx 10^{12}$, about 2% of α (see Figure 2.1(b)), as expected. The bifurcation diagram restricted on the center manifold is depicted in Figure 2.2(a), with the corresponding bifurcation diagram in the original system projected in the α-r plane as shown in Figure 2.2(b). It should be noted that the scaling between the graphs in Figures 2.2(a) and 2.2(b) depends on the transformation matrix T_s. Also, note that the upper half branch in Figure 2.2(a) (denoted by the solid line) indicates that it is stable but is only restricted to the 1-dimensional center manifold. For the whole system, this branch is still unstable since the system contains an unstable manifold (as shown in Figure 2.2(b)).

2.3.2. Hopf bifurcation and limit cycles. To find any possible Hopf bifurcation which may occur from the infected equilibrium E_1, we first need to determine the critical points at which Hopf bifurcation occurs. The necessary and sufficient conditions for general n-dimensional systems to have a Hopf bifurcation are obtained in [43]. To state the theorem, consider the general nonlinear differential system

$$\dot{x} = f(x, \alpha), \quad x \in \mathbb{R}^n, \ \alpha \in \mathbb{R}^m, \tag{2.10}$$

with an equilibrium determined from $f(x, \alpha) = 0$, as, say, $x_e = x_e(\alpha)$. To find the stability of x_e, evaluating the Jacobian of system (2.10) at $x = x_e(\alpha)$ yields $J(\alpha) = D_x f|_{x=x_e(\alpha)} = \left[\frac{\partial f_i(x_e(\alpha),\alpha)}{\partial x_j}\right]$. The eigenvalues of the Jacobian $J(\alpha)$ are determined by the following characteristic polynomial:

(2.11)
$$\begin{aligned} P_n(\lambda) &= \det[\lambda I - J(\alpha)] \\ &= \lambda^n + a_1(\alpha)\,\lambda^{n-1} + a_2(\alpha)\,\lambda^{n-2} + \cdots + a_{n-2}(\alpha)\,\lambda^2 + a_{n-1}(\alpha)\,\lambda + a_n(\alpha). \end{aligned}$$

Then, by the Hurwitz criterion [21], we know that the equilibrium solution $x_e(\alpha)$ is asymptotically stable if and only if all the roots of the polynomial $P_n(\lambda)$ have negative real part, or equivalently, if and only if all the following Hurwitz arrangements $\Delta_i(\alpha)$ $(i = 1, 2, \ldots, n)$ are positive:

$$\Delta_1 = a_1, \quad \Delta_2 = \det\begin{bmatrix} a_1 & 1 \\ a_3 & a_2 \end{bmatrix}, \quad \Delta_3 = \det\begin{bmatrix} a_1 & 1 & 0 \\ a_3 & a_2 & a_1 \\ a_5 & a_4 & a_3 \end{bmatrix}, \quad \ldots \quad \Delta_n = a_n \cdot \Delta_{n-1}.$$

Having defined the Hurwitz arrangements as above, we have the following theorem.

THEOREM 1 (see [43]). *The necessary and sufficient condition for a Hopf bifurcation to occur from the equilibrium solution $x_e(\alpha)$ of system* (2.10) *is $\Delta_{n-1} = 0$, with $a_n > 0$ and $\Delta_i > 0$, for $1 \le i \le n-2$.*

In order to further consider the postcritical dynamical behavior of the system and to determine the stability of bifurcating limit cycles, we may apply normal form theory to system (2.10). Assume that at a critical point $\alpha = \alpha_c$, the Jacobian of (2.10) evaluated at the equilibrium x_e contains a pair of purely imaginary eigenvalues $\pm i\omega_c$, and all other eigenvalues have negative real part. Then, the normal form of system (2.10) associated with Hopf bifurcation can be written in polar coordinates as (see, e.g., [42])

$$\frac{d\rho}{dt} = \rho\,\left(v_0\,\mu + v_1\,\rho^2 + \cdots\right), \quad \frac{d\theta}{dt} = \omega_c + t_0\,\mu + t_1\,\rho^2 + \cdots, \tag{2.12}$$

where $\mu = \alpha - \alpha_c$, ρ and θ denote the amplitude and phase of motion, respectively. Then, the first equation of (2.12) can be used to approximate the amplitude of bifurcating limit cycles and to determine their stability. The second equation of (2.12) can determine the frequency of periodic motion. The coefficient v_1, usually called the first-order focus value, plays an important role in determining the stability of limit cycles. When $v_1 < 0$ ($v_1 > 0$, respectively), the Hopf bifurcation is called supercritical (subcritical) and the bifurcating limit cycles are stable (unstable). The Maple program developed in [42] can be easily applied to system (2.10) to obtain the normal form (2.12). The coefficients v_0 and t_0 for the linear part of system (2.10) can be found from a linear analysis, given by [44], $v_0 = \frac{1}{2}(a_{11} + a_{22})$, $t_0 = \frac{1}{2}(a_{12} - a_{21})$, where $a_{ij} = \frac{\partial f_i}{\partial x_j \partial \mu}$, evaluated at the critical point.

We now apply the above formula to consider the infected equilibrium E_1 of system (2.10). To check if there exists a Hopf bifurcation from E_1, based on the 4th-degree characteristic polynomial $P_1(\xi, r_{e1})$, we apply the formula $\Delta_3 = a_1a_2a_3 - a_3^2 - a_1^2a_4 = 0$ and solve this equation for r to obtain a unique value, $r_H > 0$, such that (by using (2.9)) $\alpha_H = \alpha_1(r_H) > 0$. When the parameter values in Table 2.1 are used, these critical values are given by $(r_H, \alpha_H) \approx (6.72\times10^{13}, 2.64\times10^{13})$, at which the Jacobian of system (2.1) contains a purely imaginary pair and two negative real eigenvalues $\pm 0.308\, i$, -1.66, and -3.66×10^7. Thus, as α is varied across α_H, a Hopf bifurcation occurs from E_1, leading to a family of limit cycles.

To find the approximate solutions of the limit cycles and to determine their stability, we apply normal form theory to this model associated with this singularity. First, we apply a transformation $(x, y, r, a)^T = (x_{e1}, y_{e1}, r_{e1}, a_{e1})^T + T_H\,(x_1, x_2, x_3, x_4)^T$, where $(x_{e1}, y_{e1}, r_{e1}, a_{e1})$ is the infected equilibrium solution E_1 and T_H is a constant, nonsingular matrix. We obtain a transformed system of (2.1), which we omit due to its lengthy expression. Then, applying the formulas $v_0 = \frac{1}{2}(a_{11}+a_{22})$, $t_0 = \frac{1}{2}\,(a_{12}-a_{21})$ to the transformed system, we obtain $v_0 \approx 3.15 \times 10^{-15}$ and $t_0 \approx 3.33 \times 10^{-15}$. Further, we apply the Maple program [42] to the transformed system to obtain $v_1 \approx -4.18\times10^{-7}$ and $t_1 \approx -3.38\times10^{-6}$. Thus, the normal form up to third order is given by

$$\begin{aligned} \frac{d\rho}{dt} &\approx \rho(3.15\times10^{-15}\mu - 4.18\times10^{-7}\rho^2 + \cdots), \\ \frac{d\theta}{dt} &\approx 0.308 + 3.33\times10^{-15}\mu - 3.38\times10^{-6}\rho^2 + \cdots . \end{aligned} \tag{2.13}$$

The first equation of (2.13) can be used to analyze the bifurcation and stability of bifurcating limit cycles. Setting $\frac{d\rho}{dt} = 0$ results in two solutions: $\rho = 0$, which represents the infected equilibrium solution E_1; and $\rho \approx 8.68\times10^{-5}\sqrt{\mu}$ $(\mu > 0)$, which is an approximation of the amplitude of bifurcating limit cycles. Since $v_1 < 0$, this is a supercritical Hopf bifurcation, and bifurcating limit cycles are stable. For example, choose $\mu = 10^{12}$. Then, the approximate amplitude of the limit cycle is $\rho \approx 86.8$, and the frequency of the limit cycle approximately equals $\omega \approx 0.283$, slightly less than $\omega_c \approx 0.308$. The phase portrait of the simulated limit cycle, projected on the x-y plane, is shown in Figure 2.3(d). It can be seen from Figures 2.3(a) and (d) that the analytical prediction from the normal form, $\rho \approx 86.8$, agrees well with the simulated result.

The above analysis based on normal form theory is for local dynamical behavior; that is, the limit cycles must be near the Hopf critical point (r_H, α_H). It can be seen from Figure 2.1(b) that values of α taken from the interval $\alpha \in (\alpha_H, \alpha_t)$ lead to unstable equilibrium solutions (since both E_0 and E_1 are unstable for this interval). However, due to the solutions being nonnegative and bounded, we expect that there should exist certain persistent motions such as oscillating solutions for the values of α taken from this interval, and the amplitudes of these oscillations can be large. For example, for $\alpha = 3.50\times10^{13}$, the phase portrait of the simulated solution, projected on the x-y plane, is shown in Figure 2.3(e), corresponding to the oscillations in time shown in Figure 2.3(b), which have much greater amplitude than the oscillations in Figure 2.3(a).

Now, we take a particular value of α from the interval $\alpha \in (\alpha_H, \alpha_t)$, which is close to α_t, to simulate the system. For example, taking $\alpha = 4.55\times10^{13} < \alpha_t \approx 4.58\times10^{13}$, we obtain the phase portrait of the simulated oscillating solution, projected on the x-y plane, shown in Figure 2.3(f) with corresponding time history of x and y shown in Figure 2.3(c). This clearly shows viral blips.

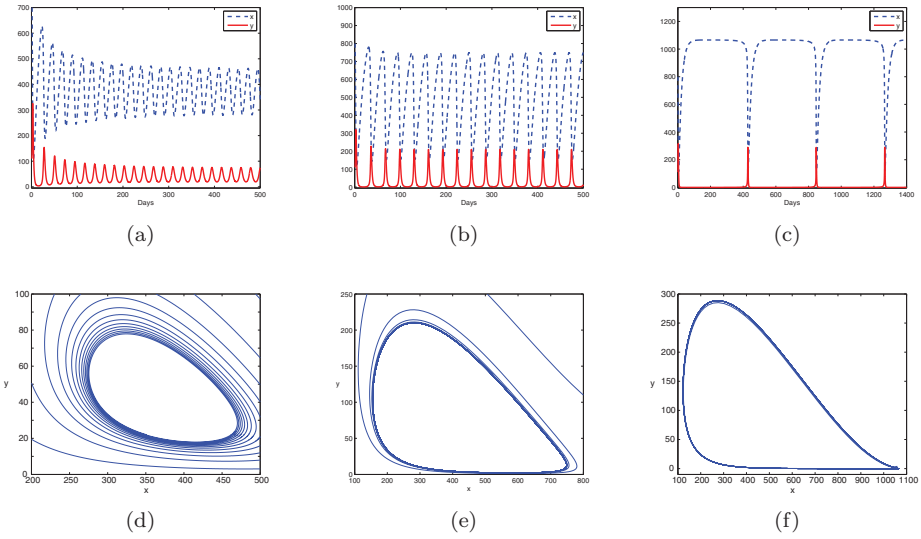

FIG. 2.3. *Simulated limit cycles of system* (2.1) *for the parameter values taken from Table* 2.1*, with the time course of* x *and* y *on the top row and the corresponding phase portraits projected on the* x*-*y *plane on the bottom row. For* (a) *and* (d) $\alpha = 2.74 \times 10^{13}$*, for* (b) *and* (e) $\alpha = 3.50 \times 10^{13}$*, and for* (c) *and* (f) $\alpha = 4.55 \times 10^{13}$.

Next, we will discuss what conditions are needed for creating the phenomenon of viral blips.

2.4. Conditions for generating viral blips. In the previous subsection, we carefully analyzed the occurrence of viral blips in a 4-dimensional HIV model (2.1). System (2.1) is an example of an *in-host infection model*, an ODE system describing the dynamics of infection within a single infected individual. In-host infection models, based on classical susceptible-infected-recovered (SIR) models in epidemiology [1], typically include populations of uninfected target cells, infected target cells, and the infection dynamics between the two classes [28]. More complex models also include populations of free virus, latently infected cells, and various relevant components of the immune response, depending on the infection under study. Although there are many exceptional cases, in-host models typically admit an uninfected equilibrium and at least one infected equilibrium, analogous to the disease-free and endemic equilibria of an SIR model.

Since in-host infection models share many similar features, much of our understanding regarding the behavior of system (2.1) can be generalized to other models. Based on insights obtained in analyzing system (2.1), we propose in the following hypothesis four conditions for an in-host infection model to generate viral blips.

Hypothesis 1. The following conditions are needed for an in-host infection model to generate viral blips:

(i) there exist at least two equilibrium solutions;
(ii) there exists a transcritical bifurcation at an intersection of the two equilibrium solutions;
(iii) there is a Hopf bifurcation which occurs from one of the equilibrium solutions; and
(iv) large oscillations (or, more generally, global, persistent motions) can occur

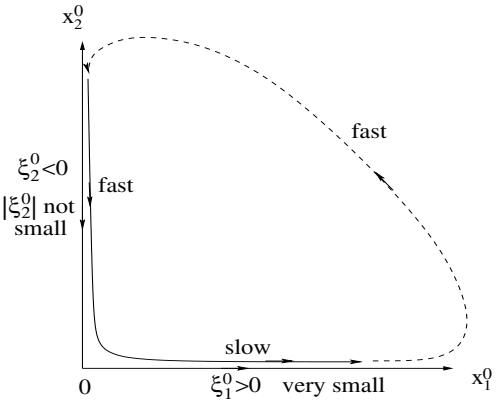

FIG. 2.4. *Schematic diagram for explaining the occurrence of blips.*

near the transcritical critical point.

The reasons for conditions (i) and (ii) are simple because when a parameter that reflects infection severity is chosen as a bifurcation parameter, an in-host infection model typically starts at the uninfected equilibrium and then bifurcates to the infected equilibrium as the parameter is increased. Thus, these two equilibrium solutions must exchange their stability, yielding a transcritical bifurcation. For the 4-dimensional model considered in the previous subsection, the uninfected equilibrium E_0 and the infected equilibrium E_1 intersect at the critical point (α_t, r_t), where they exchange their stability. In fact, E_0 is stable (unstable) for $\alpha > \alpha_t$ ($\alpha < \alpha_t$), while the lower branch of E_1 is stable (unstable) for $\alpha < \alpha_t$ ($\alpha > \alpha_t$), as shown in Figure 2.1(b).

Condition (iii), the existence of a Hopf bifurcation, is necessary to obtain oscillations. It can be seen from Figure 2.1(b) that limit cycles bifurcate from E_1 at the Hopf critical point (α_H, r_H), and the limit cycles become larger if $\mu = \alpha - \alpha_H > 0$ increases.

The reasoning behind condition (iv) is not so obvious. Large oscillations (or global, persistent motions) are necessary, near the transcritical point, for viral blips to emerge. As shown in Figure 2.1(b), both E_0 and E_1 are unstable for $\alpha \in (\alpha_H, \alpha_t)$ (though a part of the lower branch of E_1 is stable, it is biologically meaningless due to $y < 0$). Thus, there exist large oscillations near the transcritical critical point α_t. Moreover, it is noted from Figure 2.1(b) that at the left side of the transcritical point α_t, the eigenvalues evaluated at E_0 are all real, containing one positive eigenvalue ($\xi_1^0 > 0$) and three negative eigenvalues ($\xi_i^0 < 0, i = 2, 3, 4$). In other words, any point on the uninfected equilibrium E_0 for $\alpha < \alpha_t$ is a saddle point. Since ξ_1^0 crosses zero at the critical point $\alpha = \alpha_t$, ξ_1^0 is very small near the critical point for $\alpha < \alpha_t$.

Now suppose we consider a value of $\alpha < \alpha_t$, but near the critical point $\alpha = \alpha_t$ (e.g., $\alpha = 0.455 \times 10^{14}$, as shown in Figures 2.3(c) and (f)). For simplicity, we may consider a submanifold whose linear part is characterized by the eigenvalues ξ_1^0 and ξ_2^0, and the corresponding coordinates are x_1^0 and x_2^0, respectively. A solution trajectory of system (2.1) for such a value of α, projected on this submanifold, is depicted in Figure 2.4. Due to $0 < \xi_1^0 \ll 1$, the trajectory moves away from the critical point very slowly near the x_1^0-axis, while it moves rapidly toward the critical point near the x_2^0-axis since $|\xi_2^0|$ is not small. Further, due to the global boundedness of solutions, the part of the trajectory which is not close to the saddle point moves rapidly, as shown in Figure 2.4. This fast-slow motion yields the blips phenomenon, with slow

changes corresponding to the near-flat section in the time history, and rapid changes occurring during the viral blips, as shown in Figures 2.3(c) and (f). In other words, the trajectory spends relatively long periods in regions of state space which lie very close to the uninfected equilibrium and then transiently visits regions of state space which are close to the infected equilibrium.

3. A simple 3-dimensional in-host infection model producing blips. Having established the conditions in Hypothesis 1 for generating viral blips, we are ready to turn to some basic questions such as the following: What types of in-host infection models can generate blips, and what is the minimum dimension of such models?

3.1. Generalizing ROS to other physical variables. In model (2.1), the variable r represents ROS, which are produced naturally in the body. In HIV infection, extra ROS are generated by infected cells, and these in turn directly accelerate HIV progression [29, 36]. Therefore, infectivity β is an increasing and saturating function of ROS concentrations. However, we note that the form of the infection term is not specific to HIV or to ROS, and models of a similar form could in fact apply to other infections. To generalize the physical meaning of the variable r, we can, for example, let r denote any damage caused by the infection, for example, to the humoral immune response, to infected organs, or to the infected individual aspecifically. The model assumes that "damage" increases with the extent of the infection at rate ky and is repaired or cleared at rate $d_r r$. This yields the 3-dimensional system

$$\dot{x} = \lambda_x - d_x x - \beta(r)xy, \qquad \dot{y} = \beta(r)xy - d_y y, \qquad \dot{r} = ky - d_r r. \tag{3.1}$$

To achieve an infection term similar to that in model (2.1), we further assume that accrued damage makes target cells more vulnerable to infection, that is, that accrued damage increases the infection rate. We thus take $\beta(r)$ to be an increasing, saturating function of r.

In the original model (2.1), r represents ROS, for example, H_2O_2, whose production and decay rates are both extremely fast. For the more general model (3.1), we would like to assess whether viral blips are still possible at more moderate production and repair rates, k and d_r. For ROS the decay rate $d_r = 1.66 \times 10^7\,\mathrm{day}^{-1}$ implies a half life of only 4ms. We decreased d_r by several orders of magnitude; in particular, at $d_r = 1.0 \times 10^3\,\mathrm{day}^{-1}$, a half life of 60s, we find that viral blips are still possible. For this value of d_r, we can take $k = 1.49 \times 10^{15}\,\mathrm{molecules\,cell}^{-1}\,\mathrm{day}^{-1}$. Note that λ_r has been set to zero in (3.1) to make the model more general.

For simplicity, let $a = b_{\max} - b_0$, $b = b_0$, and $c = r_{\mathrm{half}}$. Then, the function $\beta(r)$ is rewritten as $\beta(r) = b + \frac{a\,r}{r+c}$, and a, b, and c are treated as bifurcation parameters. Parameter values λ_x, d_x, d_y, k, d_r, b_0, $b_{\max}$, and r_{half} are given in Table 2.1. For practically meaningful solutions, the values of the bifurcation parameters will be chosen close to the values in Table 2.1.

To analyze (3.1), we can follow the same procedure used in the previous section and treat b as a bifurcation parameter. First, it is easy to prove the well-posedness of system (3.1). Next, we get the infection-free equilibrium $\mathrm{E}_0 : (x_{e0}, y_{e0}, r_{e0}) = (\lambda_x/d_x, 0, 0)$ and the infected equilibrium $\mathrm{E}_1 := (x_{e1}, y_{e1}, r_{e1})$, where $x_{e1} = \frac{d_y(r_{e1}+c)}{(a+b)r_{e1}+bc}$, $y_{e1} = \frac{1}{d_y}(\lambda_x - d_x x_{e1})$, and r_{e1} is determined by $F_1(r,c) = d_r d_y (a+b) r^2 + [d_y(d_r bc + kd_x) - k\lambda_x(a+b)]\,r + kc(d_x d_y - b\lambda_x) = 0$. Again, it is easy to show that E_0 and E_1 intersect at the transcritical bifurcation point $(b_t, r_t) \approx (9.38 \times 10^{-4}, 0)$. On the infected equilibrium E_1, there are two saddle-node bifurcation points (turning points),

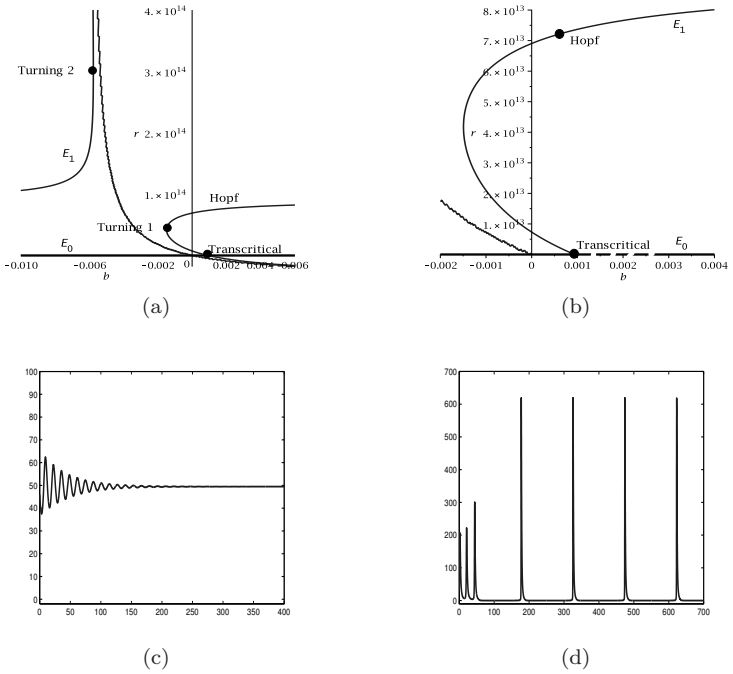

FIG. 3.1. *Dynamics and bifurcation of system* (3.1) *for* $d_r = 1.0 \times 10^3$, $k = 1.49 \times 10^{15}$*:* (a) *bifurcation diagram projected on the b-r plane;* (b) *a close-up of part* (a)*;* (c) *simulated time history* $y(t)$ *converging to* E_1 *for* $b = 0.001$ *with the initial condition* $(x, y, r) = (178, 46, 73)$ *close to* E_1*; and* (d) *simulated time history* $y(t)$ *converging to a stable limit cycle (blips) for* $b = 0.001$ *with the initial condition* $(x, y, r) = (1005, 3, 3)$ *close to* E_0.

$(b_{s_1}, r_{s_1}) \approx (-1.49 \times 10^{-3}, 4.18 \times 10^{13})$ and $(b_{s_2}, r_{s_2}) \approx (-5.77 \times 10^{-3}, 3.05 \times 10^{14})$, and a Hopf bifurcation point $(b_H, r_H) \approx (6.56 \times 10^{-4}, 7.24 \times 10^{13})$.

The bifurcation diagram and simulated results are shown in Figure 3.1. All the conditions (i)–(iv) in Hypothesis 1 are satisfied. Blips do appear since the Hopf critical point is close to the transcritical point. However, because E_0 is not globally stable, depending on the initial conditions, the oscillation may converge to the stable equilibrium E_1 (see Figure 3.1(c)) or converge to a limit cycle with large amplitude (blips), as shown in Figure 3.1(d). Convergence to a smaller, regular oscillation due to the Hopf bifurcation is also possible (not shown in Figure 3.1).

3.2. Identifying the region of parameter space exhibiting viral blips. Having found viral blip behavior in the simple 3-dimensional infection model (3.1), we are now further interested in identifying the region of parameter space in which viral blips may occur. This is particularly useful in applications since in reality, all parameters are roughly measured. Thus, we need to study the robustness of the phenomenon to variations in the system parameters. If blips appear only for a very small region in the parameter space, then the results are not practically useful. The main idea of identifying the region where blips may occur is to study the instability of the solutions of the system. Once the unstable region is identified, blips can be found by using the other conditions in Hypothesis 1. In order to simplify the analysis, we first introduce state variable scaling and parameter rescaling into system (3.1).

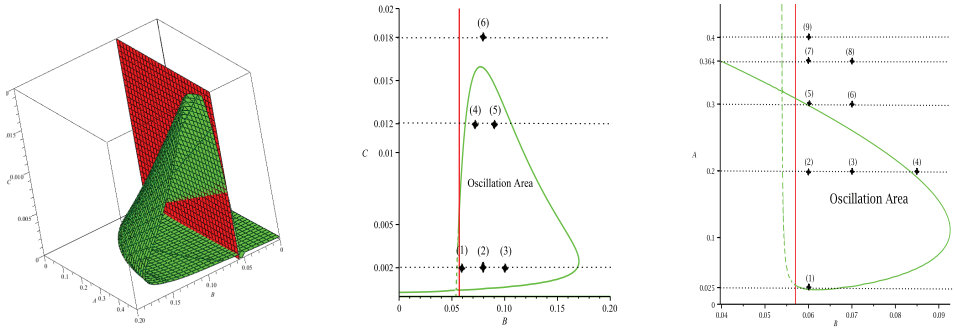

(a) (b) (c)

FIG. 3.2. (a) *Graph of* $\Delta_2 = 0$ *in the A-B-C parameter space, identifying the region yielding oscillations;* (b) *cross section of panel* (a) *where* $A = 0.364$*; and* (c) *cross section of panel* (a) *where* $C = 3.94 \times 10^{-4}$.

3.2.1. State variable scaling and parameter rescaling. Introducing the scaling $x = c_1 X$, $y = c_2 Y$, $r = c_3 R$, $t = c_4 \tau$, where $c_1 = \frac{\lambda_x}{d_y}$, $c_2 = \frac{\lambda_x}{d_y}$, $c_3 = \frac{\lambda_x k}{10^{13} d_y^2}$, $c_4 = \frac{1}{d_y}$, to (3.1) and letting $A = \frac{a\,\lambda_x}{d_y^2}$, $B = \frac{b\,\lambda_x}{d_y^2}$, $C = \frac{c\,d_y^2}{10^{12}\lambda_x\,k}$, $D_x = \frac{d_x}{d_y}$, $D_r = \frac{d_r}{d_y}$ yields the scaled system

(3.2)
$$\dot{X} = 1 - D_x X - \left(B + \frac{AR}{R+C}\right) XY, \quad \dot{Y} = \left(B + \frac{AR}{R+C}\right) XY - Y, \quad \dot{R} = Y - D_r R,$$

which will be used in the following analysis, with the scaled parameter values given by

(3.3)
$$A = 0.364, \quad C = 3.94 \times 10^{-4}, \quad D_x = 0.057, \quad D_r = 1000,$$

and with B treated as a bifurcation parameter.

3.2.2. Equilibrium solutions and their stability. The bifurcation patterns of the scaled system (3.2) are the same as those of system (3.1). Two equilibrium solutions are $E_0 : (X_{e0}, Y_{e0}, R_{e0}) = (1/D_x, 0, 0)$, and $E_1 : (X_{e1}, Y_{e1}, R_{e1})$, where $X_{e1} = \frac{R_{e1}+C}{(A+B)R_{e1}+BC}$, $Y_{e1} = 1 - \frac{D_x(R_{e1}+C)}{(A+B)R_{e1}+BC}$, and R_{e1} is determined from the equation $F_3(R) = D_r(A+B)R^2 + [D_r BC + D_x - (A+B)]R + (D_r - B)C = 0$.

The characteristic polynomial for E_0 is $P_0(\xi) = (\xi + D_x)(\xi + D_r)(\xi - \frac{B}{D_x})$. It is easy to show that E_0 and E_1 exchange stability at the transcritical bifurcation point $B = D_x$. The characteristic polynomial for E_1 is $P_1(\xi) = \xi^3 + a_1(r)\xi^2 + a_2(r)\xi + a_3(r)$, and the Hopf critical point is determined by $\Delta_2 = a_1(r)\,a_2(r) - a_3(r) = 0$. We fix parameters D_r and D_x and choose A, B, and C as bifurcation parameters. Then we want to find the parameter region where blips may occur. First, a Hopf bifurcation is necessary, requiring the condition $\Delta_2(A, B, C) = 0$. The graph of $\Delta_2(A, B, C) = 0$ is plotted in the 3-dimensional A-B-C parameter space, as shown in Figure 3.2(a), where the green hypersurface defines a set of points which are Hopf critical points; and the region bounded by the green surface is unstable for E_1, leading to oscillations. Thus blips may occur within this region and near the boundary as well, depending on the relative position of the Hopf critical point with respect to the transcritical point.

In the following, we fix either parameter A or parameter C to obtain two-dimensional graphs, which illustrate more clearly the bifurcations necessary for blips.

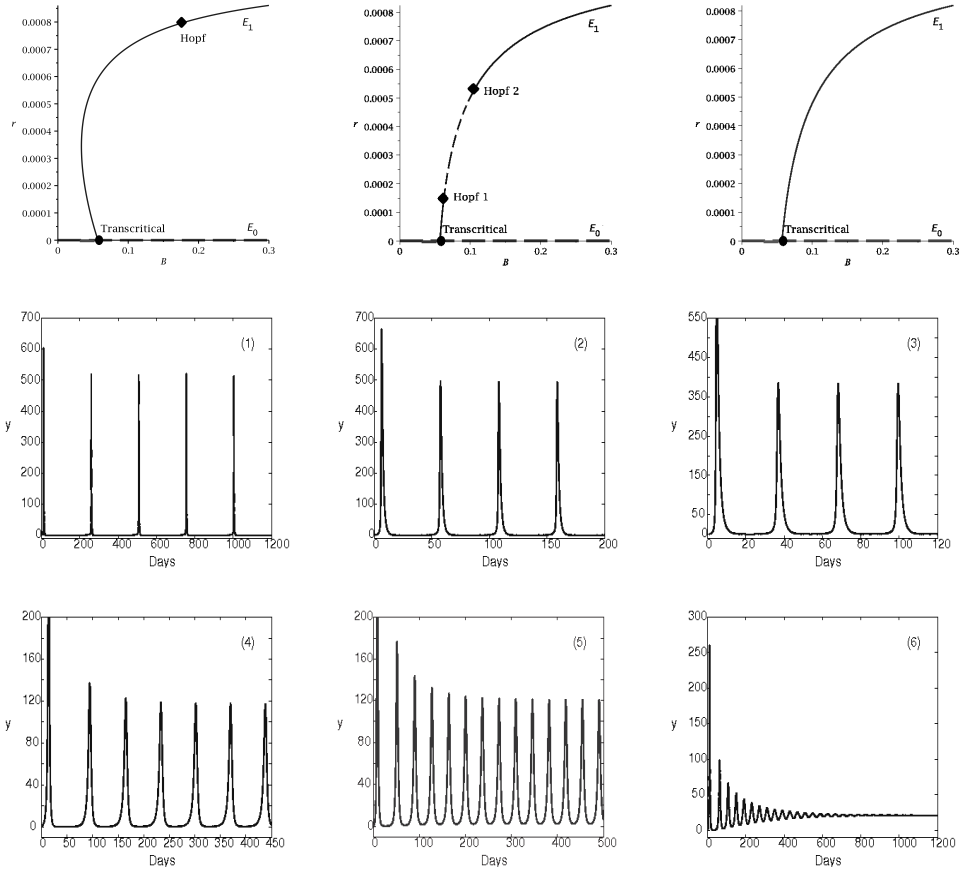

FIG. 3.3. *Bifurcation diagrams corresponding to* $C = 0.002, 0.012,$ *and* 0.018*, respectively, and numerical simulation results for the parameter values* $(B, C) = (0.06, 0.002)^{(1)}$*,* $(0.08, 0.002)^{(2)}$*,* $(0.10, 0.002)^{(3)}$*,* $(0.07, 0.012)^{(4)}$*,* $(0.09, 0.012)^{(5)}$*,* $(0.08, 0.018)^{(6)}$*.*

3.2.3. Parameter *A* fixed. Fix $A = 0.364$, which cuts the surface in Figure 3.2(a) to yield curves, as shown in Figure 3.2(b). The transcritical bifurcation occurs at $B = 0.057$, which is denoted by a red line in Figure 3.2(b). A Hopf bifurcation occurs on the green curve, and the region bounded by the green and red curves indicates where oscillations can happen. It should be noted that the above results are based on local dynamical analysis; thus blips may also appear outside this bounded region but close to the green curve.

We take three typical values of C (as the three dotted lines shown in Figure 3.2(b)), and we obtain the Hopf critical points as follows:

$$\begin{aligned} C = 0.002: &\quad (B_H, R_H) \approx (1.69 \times 10^{-1},\ 7.90 \times 10^{-4}),\\ C = 0.012: &\quad (B_{H_1}, R_{H_1}) \approx (6.27 \times 10^{-2},\ 1.53 \times 10^{-4}),\\ C = 0.012: &\quad (B_{H_2}, R_{H_2}) \approx (1.06 \times 10^{-1},\ 5.31 \times 10^{-4}),\\ C = 0.018: &\quad \text{No Hopf critical point.} \end{aligned} \tag{3.4}$$

The bifurcation diagrams corresponding to the three lines, $C = 0.002$, $C = 0.012$, and $C = 0.018$, are shown in the top three graphs in Figure 3.3. Six simulated results are also presented in this figure, corresponding to the six points marked on

the three dotted lines in Figure 3.2(b). It is seen that the values taken from the points (1)–(4) generate blips; point (5) leads to a regular oscillation, while point (6) gives a simple stable equilibrium solution, as expected. For this case when parameter A is fixed, no blips have been found for the values outside the region bounded by the red and green curves. It should be noted in the top middle figure of Figure 3.3 that there are two Hopf bifurcation points on the equilibrium E_1. One of them is supercritical while the other is subcritical, but the two families of the limit cycles bifurcating from these two critical points are both stable, since the stability change is reversed at the two points. In fact, the three eigenvalues along the unstable part of E_1 between the two Hopf bifurcation points contain one negative eigenvalue and a pair of complex conjugates with positive real part. On the two stable parts, the real part of the complex conjugate eigenvalues changes sign to become negative. As the parameter C is increasing from 0.002 to 0.018, the two Hopf bifurcation points merge to a single point on E_1 (corresponding to the turning point on the green curve (see Figure 3.2(b)), at which the horizontal line is tangent to the green curve); the corresponding eigenvalues contain a negative eigenvalue and a purely imaginary pair. This indeed characterizes a degenerate Hopf bifurcation (see, e.g., [44]) different from the Hopf bifurcation defined by (2.12). A similar discussion applies to the other two Hopf bifurcation points shown in the top left figure in Figure 3.4.

3.2.4. Parameter C fixed. Now we fix parameter $C = 3.94 \times 10^{-4}$, which results in curves in the A-B plane by cutting the surface in Figure 3.2(a), as shown in Figure 3.2(c). The transcritical point is kept the same: $B = 0.057$. We choose three typical values of A, and we find the Hopf bifurcation points as follows:

$$
\begin{array}{ll}
A = 0.025: & (B_{H_1}, R_{H_1}) \approx (5.82 \times 10^{-2},\ 9.84 \times 10^{-5}), \\
A = 0.025: & (B_{H_2}, R_{H_2}) \approx (6.75 \times 10^{-2},\ 2.65 \times 10^{-4}), \\
A = 0.200: & (B_H, R_H) \approx (8.32 \times 10^{-2},\ 7.33 \times 10^{-4}), \\
A = 0.364: & (B_H, R_H) \approx (3.99 \times 10^{-2},\ 7.99 \times 10^{-4}).
\end{array} \tag{3.5}
$$

The bifurcation diagrams corresponding to the three lines $A = 0.025$, $A = 0.200$, and $A = 0.364$ are shown in the top three graphs in Figure 3.4. Nine simulated results are also presented in this figure, corresponding to the nine points marked on the five dotted lines in Figure 3.2(c). It is observed from these graphs that among the nine chosen parameter values, seven cases exhibit blips (see the points (2)–(7) and (9) in Figure 3.2(c) with the corresponding simulated results shown in Figure 3.4). It is noted that some of these points are not even close to the red line, nor are they in the region bounded by the red and green curves, suggesting that a simple 3-dimensional HIV model can generate rich blips.

3.3. 3-dimensional immunological model. In this subsection, we briefly consider an immunological model [28] and apply Hypothesis 1 to show that the model can have blips. For simplicity, the original 4-dimesional model is reduced (by a quasi–steady state assumption on the virus particles) to a 3-dismensional model, described by

$$
\begin{aligned}
\dot{x} &= \lambda - dx - \beta(y)xy, \\
\dot{y} &= \beta(y)xy - ay - pyz, \\
\dot{z} &= cyz - bz,
\end{aligned} \tag{3.6}
$$

where x, y, and z represent the densities of the infected cells, uninfected cells, and CTL, respectively. The system (3.6) with constant $\beta(y)$ is well known [2, 27] and

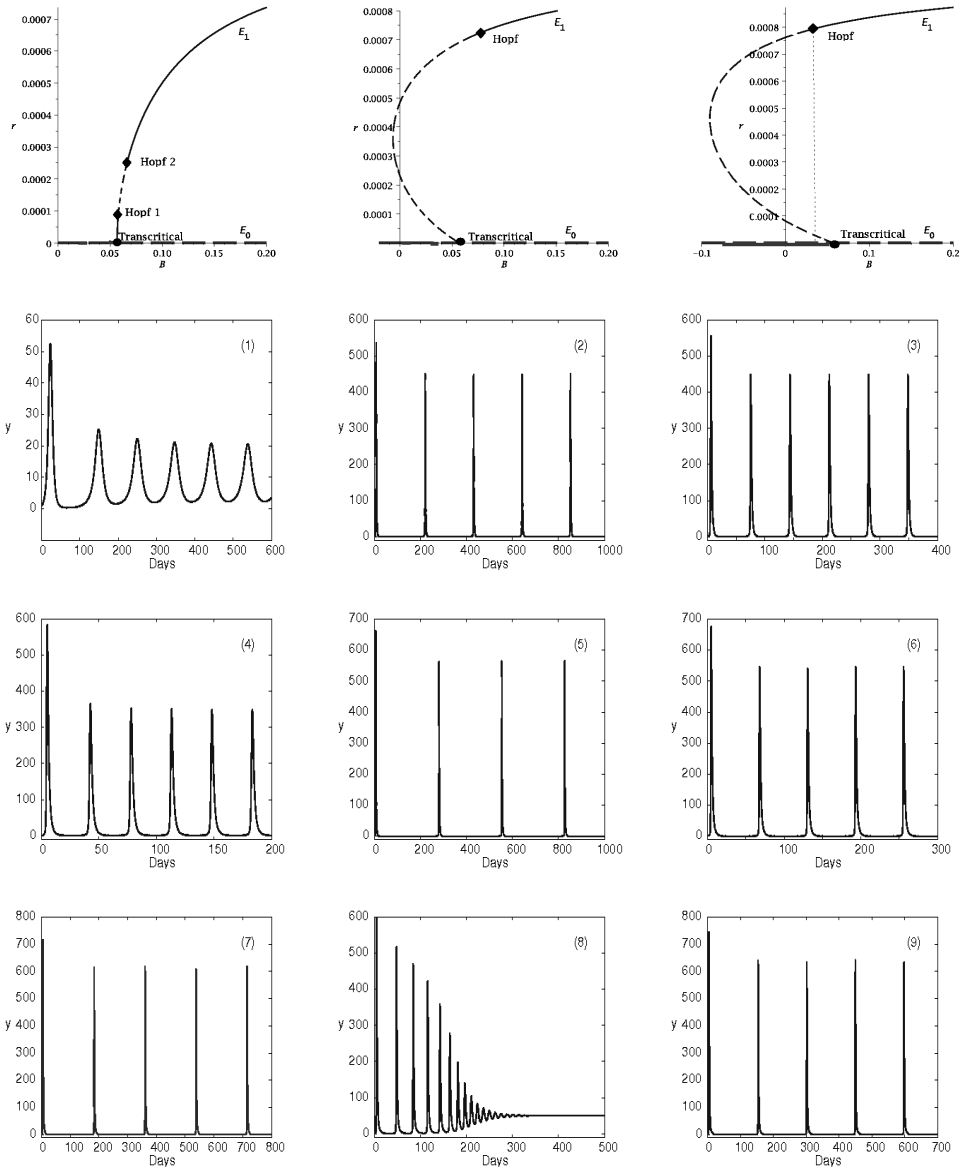

FIG. 3.4. *Bifurcation diagrams corresponding to* $A = 0.025, 0.200, 0.364$, *and numerical simulation results for the parameter values* $(A, B) = (0.025, 0.060)^{(1)}$, $(0.200, 0.060)^{(2)}$, $(0.200, 0.070)^{(3)}$, $(0.200, 0.085)^{(4)}$, $(0.300, 0.059)^{(5)}$, $(0.300, 0.070)^{(6)}$, $(0.364, 0.060)^{(7)}$, $(0.364, 0.070)^{(8)}$, $(0.400, 0.060)^{(9)}$.

does not exhibit blips. In order to generate viral blips, here we choose $\beta(y) = n + \frac{my}{y+k}$, where n and m are minimum and maximum infectivity, and k represents the density of infected cells when the infectivity takes its median value. Since the analysis is similar to previous models, we omit the details and give only the results as follows. The system (3.6) has three equilibrium solutions: the infection-free equilibrium, E_0, the infected equilibrium with CTL, E_1, and the infected equilibrium without CTL, E_2. There are two transcritical bifurcation points. One, named "transcritical 1" in

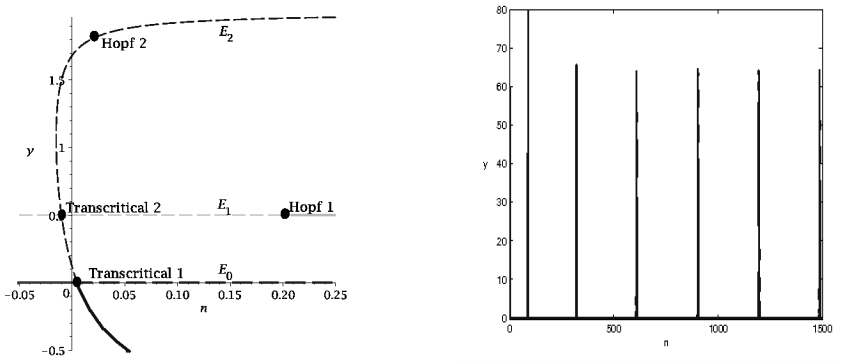

FIG. 3.5. (a) *Bifurcation diagram of system* (3.6)*, showing the equilibrium solutions* E_0*,* E_1*, and* E_2 *with dashed and solid lines denoting unstable and stable, respectively.* (b) *Simulated viral blips in system* (3.6) *for* $n = 0.007$*. Other parameter values used here are* $\lambda = k = p = 1$*,* $d = 0.01$*,* $m = b = 0.05$*,* $a = 0.5$*,* $c = 0.1$*.*

Figure 3.5(a), is at the intersection of E_0 and E_2: $(n_{t1}, y_{t1}) \approx (0.005, 0)$, at which E_0 and E_2 exchange their stability. The second occurs at the intersection of E_1 and E_2: $(n_{t2}, y_{t2}) \approx (-0.01, 0.5)$, called "transcritical 2" in Figure 3.5(a). However, note that they only exchange their stability if restricted to a one-dimensional manifold, and both of them are unstable in the whole space since one of the eigenvalues stays positive when crossing this transcritical point. E_1 becomes stable until n is increased to cross a Hopf critical point (called "Hopf 1" in Figure 3.5(a)): $(n_{1H}, y_{1H}) \approx (0.206, 0.5)$. Another Hopf bifurcation point (called "Hopf 2" in Figure 3.5(a)) happens on E_2 at $(n_{2H}, y_{2H}) \approx (0.0213, 1.81)$. The limit cycles bifurcating from Hopf 1 are stable, while those from Hopf 2 are unstable, leading to large oscillating motions when the values of n are chosen from the interval (n_t, n_{2H}). The above results show that all four conditions in Hypothesis 1 are satisfied, and blips indeed appear. The simulated blips for $n = 0.007$ are depicted in Figure 3.5(b).

4. A 2-dimensional in-host infection model. For the generalized 3-dimensional model discussed in section 3, we assume that r is some form of damage to the host or to the host immune system, which increases with the extent of the infection, that is, in proportion to the infected cell density. Here, we further assume that there is a quasi-steady state (as used in (3.1)) between the damage, r, and the infected cell density y. Thus, the 3-dimensional HIV model can be further reduced to a 2-dimensional model, given by

$$\dot{x} = \lambda_x - d_x x - \beta(y)xy, \qquad \dot{y} = \beta(y)xy - d_y y. \tag{4.1}$$

Note that system (4.1) is now in the form of an in-host infection model, which includes only uninfected and infected target cell populations and the most basic "birth" and death rates. However, we now think of the infectivity $\beta(y)$ as a possible function of y; other parameters have the same meaning as in (3.6). We will show that this simplified 2-dimensional infection model may also be able to generate blips.

4.1. 2-dimensional in-host model with constant and linear infection rates. First, we consider the case when the infection rate, $\beta(y)$, is simply a constant function; that is, $\beta(y) = \beta$. Taking β itself as a bifurcation parameter, it is easy to

show that there exist two equilibrium solutions and a transcritical bifurcation point, but no Hopf bifurcation exists. This violates Hypothesis 1, and therefore no blips can appear in this case.

Next, suppose the infection rate $\beta(y)$ is a linear function of the infected cell density, y, that is, $\beta(y) = b + ay$, where the parameters a and b represent the same constants as before, and a is treated as a bifurcation parameter. In this case, we have two equilibrium solutions E_0 and E_1. But E_0 is always stable for all values of a though there exists a Hopf bifurcation on E_1. Therefore, no transcritical bifurcation point exists for this case, which violates Hypothesis 1, implying that blips are not possible when $\beta(y)$ is a linear function.

4.2. A 2-dimensional in-host model with saturating infection rate. Motivated by our previous results for the 3- and 4-dimensional models, we next assume that infectivity is an increasing saturating function of the infected cell density, y, namely, $\beta(y) = b + \frac{ay}{y+c}$. For our numerical work, we take the same values of a and b as used in section 3.1, while c is taken to be $c = 50$, obtained by numerical simulation based on the experimental data given in [39]. Other parameter values are as described for model (3.1).

4.2.1. Scaling. For convenience in the following analysis, we first simplify system (4.1) by the following scaling to reduce the number of parameters. Let $x = e_1X$, $y = e_2Y$, $t = e_3\tau$, where $e_1 = \frac{\lambda_x}{d_y}$, $e_2 = \frac{\lambda_x}{d_y}$, $e_3 = \frac{1}{d_y}$, and set $A = \frac{a\lambda_x}{d_y^2}$, $B = \frac{\lambda_x b}{d_y^2}$, $C = \frac{cd_y}{\lambda_x}$, $D = \frac{d_x}{d_y}$. Then, the rescaled system is given by

$$\begin{aligned} \frac{dX}{d\tau} &= 1 - DX - \left(B + \frac{AY}{Y+C}\right) XY, \\ \frac{dY}{d\tau} &= \left(B + \frac{AY}{Y+C}\right) XY - Y, \end{aligned} \tag{4.2}$$

with B treated as a bifurcation parameter. Taking the parameter values from [28], we have the scaled parameter values $A = 0.364$, $C = 0.823$, and $D = 0.057$ for system (4.2).

4.2.2. Equilibrium solutions and their stability. By setting $\dot{X} = \dot{Y} = 0$ in (4.2), we get two biologically meaningful equilibrium solutions, the uninfected equilibrium solution $\mathrm{E}_0 : (X_0, Y_0) = (1/D, 0)$ and the infected equilibrium solution $\mathrm{E}_1 = (X_1, Y_1)$, where $X_1 = \frac{Y_1+C}{(A+B)Y_1+BC}$, and Y_1 is determined by the equation $F_1 = (A+B)Y^2 + (D+BC-A-B)Y + (D-B)C = 0$. This indicates that condition (i) in Hypothesis 1 is satisfied. Similarly, it is easy to find that E_0 is stable (unstable) if $B < D$ ($B > D$).

4.2.3. Bifurcation analysis. By using the characteristic polynomials at E_0 and E_1, we can show that a transcritical bifurcation occurs at the critical point, $(Y_t, B_t) = (0, 0.057)$, which satisfies condition (ii) in Hypothesis 1. E_0 and E_1 intersect at this critical point and exchange their stability. Further, a Hopf bifurcation happens at the critical point $(B_H, Y_H) \approx (0.121, 0.811)$. E_1 is stable (unstable) on the right (left) side of the Hopf bifurcation point. Therefore, condition (iii) in Hypothesis 1 holds for this case. If we take a value of B near B_t on the side where both E_0 and E_1 are unstable, then condition (iv) in Hypothesis 1 is also satisfied and so blips occur. The bifurcation diagram is shown in Figure 4.1(a), and the simulated viral blips for $B = 0.060$ are depicted in Figure 4.1(b).

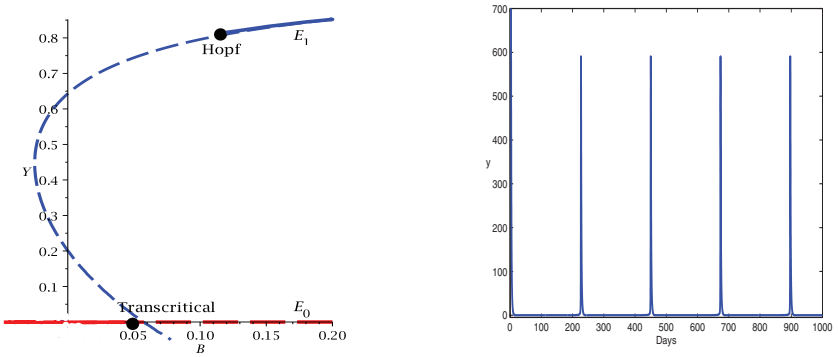

(a) (b)

FIG. 4.1. (a) *Bifurcation diagram projected on the B-Y plane, with the red and blue lines denoting the* E_0 *and* E_1*, respectively, and dotted and solid lines indicating unstable and stable, respectively.* (b) *Simulated time history of* $y(t)$ *for* $B = 0.060$.

Summarizing the results of this section, we conclude that the simple 2-dimensional in-host model is sufficiently complex to exhibit viral blips, provided the infectivity function is an increasing, saturating function of infected cell density. However, for this model, the range of parameter space in which blips occur is relatively restricted, compared with the 3-dimensional model, which is established in the previous section.

An interesting question is naturally raised here: Does there exist a more general function $\beta(y)$ such that the existence of blips depends upon the general properties of the function like its maximal values and/or its derivatives? In fact, it has been found that by choosing the parameter c large enough in the function β, a threshold is reached beyond which the Hopf bifurcation and hence also the viral blips disappear.

5. Recurrency in a 5-dimensional model. So far, we have considered 2-, 3-, and 4-dimensional in-host infection models with increasing, saturating, infectivity functions and shown that all these models exhibit blips. Moreover, it has been shown for the 2-dimensional model (and can be shown for the 3- and 4-dimensional models, but they are omitted here) that replacing the infectivity function with a constant or linear function of y will cause blips to disappear. However, in this section we will show that higher-dimensional systems may have blips even with a constant infectivity function.

We consider a previously proposed 5-dimensional immunological model in which recurrent phenomena or viral blips have been observed via numerical simulation [41]. The model describes antibody concentrations and cytotoxic T lymphocytes (CTLs) explicitly and is described as follows:

$$\dot{x} = \lambda - dx - \beta xv, \tag{5.1a}$$
$$\dot{y} = \beta xv - ay - pyz, \tag{5.1b}$$
$$\dot{z} = cyz - bz + hy, \tag{5.1c}$$
$$\dot{u} = \xi z - \eta u - kuv, \tag{5.1d}$$
$$\dot{v} = ey - kuv - \gamma xv - qv. \tag{5.1e}$$

Here x, y, z, u, and v are, respectively, the population densities of uninfected target cells, infected target cells, CTLs, antibodies, and virions. The parameters λ and dx represent the uninfected cells' constant growth rate and death rate, respectively.

TABLE 5.1
Parameter values used in model (5.1) [41].

Parameter	Value
λ	10^4 cells μL^{-1} day^{-1}
d	0.100 day^{-1}
β	1.25×10^{-5} virion^{-1} μL day^{-1}
p	10^{-4} cells^{-1} μL day^{-1}
c	10^{-4} cells^{-1} μL day^{-1}
b	0.200 day^{-1}
h	$[0, 10^{-4}]$ day^{-1}
ξ	10.0 molecules cell^{-1} day^{-1}
η	0.040 day^{-1}
k	2.50×10^{-5} particle^{-1} μL day^{-1}
e	2.50 virions cell^{-1} day^{-1}
γ	5.00×10^{-5} cell^{-1} μL day^{-1}

Target cells are infected by virus at rate βxv. The infected cells die at rate ay, being killed by CTLs at rate pyz. It is assumed that CTLs proliferate at rate cyz and decrease with the natural death rate bz. Equation (5.1d) describes the antibody growth rate, ξz, which is proportional to the number of CTLs, the natural death rate of antibody, ηu, and the binding rate of one antibody with one antigen, kuv. In (5.1e), viruses are released from infected cells at rate ey and are bound by antibody, absorbed by uninfected cells, or cleared at rates kuv, γxv, and qv, respectively. The term hy corresponds to the CTL differentiated from memory T cells [41] and should be expressed as $h_M y z_M$, where z_M is the population density of virus-specific memory T cells, which produce activated CTLs with rate $h_M y$. In [41], z_M is assumed to be a constant, and so we have $h = h_M z_M$. We will consider two cases: $h = 0$ and $h \neq 0$; $h = 0$ is due to the absence of memory T cells (that is, $z_M = 0$) during the primary effector stage. We will show the relation between the two cases. For simplicity, without loss of the properties of antibodies, we assume $q = 0$ according to [41]. Other experimental parameter values used for studying model (5.1) are given in Table 5.1.

5.1. Well-posedness of model (5.1). Due to physical meaning, negative values of the state variables of system (5.1) are not allowed. Only nonnegative initial conditions are considered, and the solutions of (5.1) must not be negative. The parameters in (5.1) are all positive due to their biological meaning. Expressing the solutions of the system (5.1) by variation of constants yields

$$x(t) = x(0)\exp\left[-\int_0^t (d+\beta v(s))\,\mathrm{d}s\right] + \lambda\int_0^t \exp\left[-\int_s^t (d+\beta v(w))\,\mathrm{d}w\right]\mathrm{d}s, \tag{5.2a}$$

$$y(t) = y(0)\exp\left[-\int_0^t (a+pz(s))\,\mathrm{d}s\right] + \beta\int_0^t x(s)v(s)\exp\left[-\int_s^t (a+pz(w))\,\mathrm{d}w\right]\mathrm{d}s, \tag{5.2b}$$

$$z(t) = z(0)\exp\left[\int_0^t (cy(s)-b)\,\mathrm{d}s\right] + h\int_0^t y(s)\exp\left[\int_s^t (cy(w)-b)\,\mathrm{d}w\right]\mathrm{d}s, \tag{5.2c}$$

$$u(t) = u(0)\exp\left[-\int_0^t (\eta+kv(s))\,\mathrm{d}s\right] + \xi\int_0^t z(s)\exp\left[-\int_s^t (\eta+kv(w))\,\mathrm{d}w\right]\mathrm{d}s, \tag{5.2d}$$

$$v(t) = v(0)\exp\left[-\int_0^t (ku(s)+\gamma x(s)+q)\mathrm{d}s\right] + e\int_0^t y(s)\exp\left[-\int_s^t (ku(w)+\gamma x(w)+q)\mathrm{d}w\right]\mathrm{d}s. \tag{5.2e}$$

THEOREM 2. *When the initial conditions are taken positive, the solutions of system* (5.1) *remain positive for* $t > 0$. *Moreover, they are bounded.*

Proof. By the initial condition $x(0) > 0$, it is easy to see from (5.2a) that $x(t) > 0\ \forall\, t > 0$. Next, we show that $y(t) > 0\ \forall\, t > 0$ by an argument of contradiction. Suppose, otherwise, that $y(t) < 0$ for some interval $t \in (t_1, t_2),\ t_1 > 0$. Since $y(0) > 0$, without loss of generality, we may assume t_1 is the first time for y to cross zero, i.e., $y(t) > 0\ \forall\, t \in [0,\, t_1)$, $y(t_1) = 0$ and $y(t) < 0\ \forall\, t \in (t_1,\, t_2)$. Thus, from (5.2e) we have $v(t_1) > 0$ due to $v(0) > 0$. On the other hand, it is seen from (5.2b) that $v(t)$ must cross zero to become negative at some $t > t_1$ since $y(t) < 0\ \forall\, t \in (t_1,\, t_2)$. So let $t = t_3$ be the first time for $v(t)$ to cross zero, i.e., $v(t_3) = 0$ and $v(t) > 0\ \forall\, t \in [t_1,\, t_3)$. Now, take $t^* = \min(t_2 - \epsilon,\, t_3)$, satisfying $t^* > t_1$, where $0 < \epsilon \ll 1$. So from the assumption we have $y(t^*) < 0$. However, on the other hand, it follows from (5.2b) that

$$\begin{aligned} y(t^*) &= y(t_1) \exp\left[-\textstyle\int_{t_1}^{t^*} (a + pz(s))\, \mathrm{d}s\right] + \beta \textstyle\int_{t_1}^{t^*} x(s)v(s) \exp\left[-\int_s^{t^*} (a + pz(w))\, \mathrm{d}w\right] \mathrm{d}s \\ &= \beta \textstyle\int_{t_1}^{t^*} x(s)v(s) \exp\left[-\int_s^{t^*} (a + pz(w))\, \mathrm{d}w\right] \mathrm{d}s > 0, \quad \text{since } v(s) > 0\ \ \forall\, t \in (t_1, t^*), \end{aligned}$$

leading to a contradiction. Hence $y(t) > 0\ \forall\, t > 0$, and it then follows from (5.2c) and (5.2e) that $z(t) > 0$ and $v(t) > 0\ \forall\, t > 0$. Finally, by the positivity of $z(t)$, (5.2d) gives $u(t) > 0\ \forall\, t > 0$.

It remains to prove that positive solutions of system (5.1) are all bounded. First, consider (5.1a), which yields $\dot{x} \leqslant \lambda - dx$. Given that the exponential functions have negative exponents, we show that $x(t)$ for $t > 0$ is bounded since as $t \to +\infty$,

$$x(t) \leq \exp\left(-\textstyle\int_0^t d\, \mathrm{d}s\right) \left[x(0) + \lambda \textstyle\int_0^t \exp\left(\int_0^s d\, \mathrm{d}u\right) \mathrm{d}s\right] = x(0)e^{-dt} + \frac{\lambda}{d}(1 - e^{-dt}) \leq \frac{\lambda}{d}.$$

Thus, denote $x_{\max} = \lim_{t\to+\infty} \sup x(t) = \frac{\lambda}{d}$. It is easy to see that $x_{\min} > 0$. Next, we add (5.1a) and (5.1b) together to obtain $\dot{x} + \dot{y} = \lambda - dx - ay - pyz \leqslant \lambda - \min(d, a)(x + y)$. Using the same boundedness argument for $x(t)$, we get $x(t) + y(t) \leqslant \frac{\lambda}{\min(d,\, a)}$ as $t \to +\infty$, and thus $y_{\max} = \lim_{t\to+\infty} \sup y(t) \leqslant \frac{\lambda}{\min(d,\, a)}$. Now consider (5.1e), yielding $\dot{v} \leqslant e y_{\max} - (\gamma x_{\min} + q)\, v$. Similarly, using the same boundedness argument for $x(t)$, we have $\lim_{t\to+\infty} v(t) \leqslant \frac{e y_{\max}}{r x_{\min} + q}$. To prove boundedness of $z(t)\ \forall\, t > 0$, we use proof by contradiction. Assume $z(t)$ is unbounded, i.e., $\lim_{t\to+\infty} z(t) \to +\infty$. Due to positivity of x, y, z, and v and boundedness of x, y, and v, it follows from (5.1b) that $\dot{y} < 0$ for $z > z^*$, or for $t > t^* > 0$ (z^* and t^* are finite), which implies $\lim_{t\to+\infty} y(t) \to 0$. Then, from (5.1c) we have $\dot{z} = (cy - b)z + hy$, so for sufficiently large t, $cy - b < 0$, and so $\dot{z}$ becomes negative (for some $z > z^*$), implying that z cannot increase unboundedly, which is a contradiction. Thus, we denote $z_{\max} = \max\{z(t),\, t \geqslant 0\}$. Finally, from (5.1d), we have $\dot{u} \leqslant \xi z_{\max} - \eta u$, which yields $u(t) \leqslant \frac{\xi z_{\max}}{\eta}$ as $t \to +\infty$. Hence, we have shown that the solutions of system (5.1) are positive and bounded. ∎

If the initial conditions have some zero elements, it is easy to see from (5.2) that solutions are nonnegative. Hence, system (5.1) is proved to be a well-posed biological model, with nonnegative and bounded solutions.

5.2. Equilibrium solutions and their stability. The following results are obtained based on the assumption $q = 0$ [41]. The equilibrium solutions of (5.1) are obtained by simply setting the vector field of (5.1) to zero. There are two equilibrium solutions, the infection-free equilibrium $\mathrm{E}_0 : (x_{e0},\, y_{e0},\, z_{e0},\, u_{e0},\, v_{e0}) = (\frac{\lambda}{d},\, 0,\, 0,\, 0,\, 0)$ and the infected equilibrium $\mathrm{E}_1 : (x_{e1},\, y_{e1}, z_{e1}, u_{e1}, v_{e1})$, where $v_{e1} = \frac{\lambda - d x_{e1}}{\beta x_{e1}}$, $z_{e1} = \frac{u_{e1}(\eta + k v_{e1})}{\xi}$, and $y_{e1} = \frac{v_{e1}(k u_{e1} + \gamma x_{e1})}{e}$. Further, with $h = 10^{-4}$ and other parameter

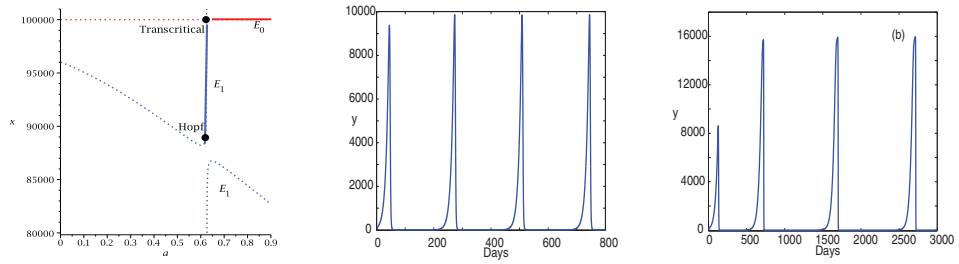

(a) (b) (c)

FIG. 5.1. *Bifurcation diagram and simulated viral blips for system* (5.1) *with the parameter values taken from Table* 5.1 *when* $a = 0.500$*:* (a) *Bifurcation diagram for* $h = 10^{-4}$*, with the red and blue lines denoting* E_0 *and* E_1*, respectively, and the dotted and solid lines indicating unstable and stable, respectively (the lower branch of* E_1 *is biologically meaningless, due to negative values in the solution);* (b) *simulated time history of* $y(t)$ *for* $h = 10^{-4}$*; and* (c) *simulated time history of* $y(t)$ *for* $h = 0$.

values taken from Table 5.1, u_{e1} can be expressed in terms of x_{e1}, and an equation $F_4(x_{e1}, a) = 0$ is obtained to determine x_{e1}.

The stability analysis for equilibria E_0 and E_1 is based on the Jacobian matrix of (5.1). Evaluating the Jacobian at the infection-free equilibrium E_0 yields the characteristic polynomial $P_{\mathrm{E}_0}(\Psi) = \det[\Psi I - J_0(\mathrm{E}_0)] = (\Psi + d)(\Psi + b)(\Psi + \eta)P_{\mathrm{E}_{0a}}$, where $P_{\mathrm{E}_{0a}} = \Psi^2 + \left(\frac{\gamma\lambda}{d} + a\right)\Psi + \frac{(a\gamma - e\beta)\lambda}{d}$. It is easy to see that the stability of E_0 is simply determined by the sign of $(a\gamma - e\beta)$; i.e., E_0 is stable (unstable) if $(a\gamma - e\beta) > 0$ (< 0). In a similar way, we evaluate the Jacobian at E_1 to obtain the 5th-degree characteristic polynomial, from which the fourth Hurwitz determinant Δ_4 can be determined.

5.3. Bifurcation analysis for $h \neq 0$. Now we consider possible bifurcations which may occur from the equilibrium solutions E_0 and E_1. First, for the infection-free equilibrium E_0, as discussed in the previous subsection, E_0 is stable (unstable) if $(a\gamma - e\beta) > 0$ (< 0). The only possible singularity occurs at the critical point, determined by $a\gamma - e\beta = 0$, at which one eigenvalue of the characteristic polynomial becomes zero (and the other four eigenvalues are negative), leading to a static bifurcation. The critical point a_{c0} is solved from $a\gamma - e\beta = 0$ as $a_{c0} = \frac{e\beta}{\gamma}$. Thus, E_0 is stable (unstable) when $a > a_{c0}$ $(a < a_{c0})$, and $x_{c0} = \frac{\lambda}{d}$. With the parameter values in Table 5.1 (with $h = 10^{-4}$), we have $(x_{c0}, a_{c0}) = (0.625, 1.00 \times 10^5)$, which actually holds for both cases $h \neq 0$ and $h = 0$.

As for the infected equilibrium E_1, one singularity happens when $a_5(x_{e1}, a)$ becomes zero. Thus, the critical point is determined by the equations $a_5(x_{e1}, a) = F_4(x_{e1}, a) = 0$, at which the characteristic polynomial of E_1 has a zero root. As a result, we obtain one biological meaningful solution, $(x_{c1}, a_{c1}) = \left(0.625, 1.00 \times 10^5\right)$. Comparing this critical point with (x_{c0}, a_{c0}) shows that these two critical points are identical, implying that E_0 and E_1 intersect and exchange their stability at this point. Denote this point as $(x_t, a_t) = (0.625, 1.00 \times 10^5)$, which is actually identical for all $h \neq 0$. The bifurcation diagram projected on the a-x plane is shown in Figure 5.1(a). It clearly shows a stability exchange between E_0 and E_1 at the transcritical point.

Now we turn to possible Hopf bifurcation from E_1. Since the characteristic polynomial P_{E_1} for E_1 cannot be factorized into polynomials of lesser degree, we will use the Routh–Hurwitz criterion to analyze its stability. The criterion states that the corresponding equilibrium is asymptotically stable if and only if all the Hurwitz

determinants are positive [4]. According to [43], the necessary condition for a Hopf bifurcation to occur from the infected equilibrium E_1 is $\Delta_4 = 0$, combined with the equation $F_4(x_{e1}, a) = 0$, since this Hopf bifurcation point is located on the infected equilibrium. Solving these two equations yields a biologically meaningful Hopf bifurcation point $(x_H, a_H) \approx (8.85\times10^4, 0.617)$. Note that the Hopf bifurcation point is above the turning point $(x_{\text{Turning}}, a_{\text{Turning}}) \approx (8.82\times10^4, 0.604)$ in the upper branch of E_1 (see Figure 5.1).

Summarizing the above results shows that the case $h \neq 0$ satisfies all four conditions in Hypothesis 1 to generate recurrent infection, and indeed recurrence occurs for $a \in (0, a^*)$, where $a^* < a_H$. Moreover, a^* should not be too close to a_H; otherwise the period of limit cycles bifurcating from the Hopf critical point (x_H, a_H) is relatively small. The bifurcation diagram, shown in Figure 5.1(a), indicates that the Hopf critical point a_H is located on the left side of $a = a_t$, where the E_0 is unstable. A simulated time course exhibiting recurrent infection is depicted in Figure 5.1(b).

5.4. Bifurcation analysis for $h \to 0^+$. Now we consider the special case, $h = 0$. It is easy to observe from (5.1c) that the solutions of system (5.1) are discontinuous at $h = 0$. Therefore, to have continuity, we should regard the special case $h = 0$ as the limiting case $h \to 0^+$. In calculation, we choose a small enough value of h (e.g., $h = 10^{-8}$) and then do the same analysis as done for the case $h \neq 0$. We also get two equilibrium solutions, the infection-free equilibrium E_0 and the infected equilibrium E_1, a transcritical bifurcation which occurs at the intersection of the two equilibria, a Hopf bifurcation emerging from the infected equilibrium E_1, and large oscillations occurring near the transcritical point on the unstable side of the Hopf critical point, given by $(x_H, a_H) \approx (8.7511\times10^4, 0.6249)$. The bifurcation diagram for this case $(h = 10^{-8})$ is similar to that shown in Figure 5.1(a), except that the two branches of E_1 are much closer, indicating that the Hopf bifurcation point moves down toward the turning point in the upper branch of E_1, which is also moving down. This implies that one branch of solution E_1 becomes an almost vertical line as $h \to 0^+$, and the Hopf critical point coincides with the turning point.

For $h = 0$, we treat it as the limit $h \to 0^+$. The seemingly vertical line in the bifurcation diagram for $h = 0$ disappears, clearly showing the discontinuity of E_1 at $h = 0$. This causes difficulty in bifurcation analysis. However, if we treat the case $h = 0$ as the limiting case $h \to 0^+$, the solution E_1 continuously depends on h, and the bifurcation diagram becomes smooth. Therefore, we can still use our theory to explain the occurrence of blips for the case $h = 0$, as shown in Figure 5.1(c). In fact, more precisely, when $h = 0$, a Bogdanov–Takens bifurcation (double-zero singularity) occurs at the point where the Hopf and turning points are merged. This is a codimension-2 bifurcation point, which in general needs two unfolding (bifurcation) parameters to give a complete local dynamical analysis. In our case, the variation of the single parameter α can be considered as a line (ray) in the two-parameter plane. It is well known that in the vicinity of a Bogdonov–Takens bifurcation point, there exist a Hopf bifurcation and a homoclinic bifurcation. Therefore, the motion generated near the codimension-2 bifurcation point may be due to either the Hopf or the homoclinic bifurcation. With respect to the blips phenomenon, the motion is large (not the small motions bifurcating from Hopf or homoclinic bifurcations) and is a globally persistent motion, and so it is not directly related to the Hopf or homoclinic bifurcations. In other words, we are more interested in possible large motions near the transcritical point.

6. Conclusion and discussion. In this paper, the problem of recurrent infection (viral blips) in in-host infection models is studied via the qualitative analysis of dynamical systems. A 4-dimensional HIV antioxidant-therapy model [39], which produces viral blips, is investigated in detail using bifurcation theory. A hypothesis consisting of four conditions for the emergence of viral blips is proposed. These conditions describe two equilibrium solutions which intersect at a transcritical bifurcation point, with a Hopf bifurcation which originates from the equilibrium solution. Under these conditions, blips appear for values of the bifurcation parameter near the transcritical point, where equilibrium solutions are unstable.

Guided by the proposed hypothesis, we propose several simpler in-host infection models that can also generate viral blips. We develop a 3-dimensional in-host model with an increasing, saturating, infection rate similar to the HIV antioxidant-therapy model and show that all four conditions in the hypothesis are satisfied, leading to blips. Further, stability and bifurcation analyses determine all possible regions in parameter space where blips may occur. We then investigate an even simpler 2-dimensional in-host model. This very simple model can also exhibit blips, as long as the infection rate is an increasing, saturating function of infected cell density. We also apply the hypothesis to study a standard HIV model with CTL response [28] and find blips by using an increasing, saturating, infection rate function.

Overall, our results suggest that simple ODE models of in-host infection dynamics are sufficient to describe transient periods of high viral replication, separated by long periods of quiescence. Rather than needing an exogenous trigger such as stochastic stimulation of the immune system, the natural dynamics of such systems may be sufficiently rich, in many cases, to exhibit viral blips. One key to obtaining this rich behavior is to propose an infection rate which increases, but saturates, with the extent of the infection. This is a natural assumption if the infection itself (high density of infected target cells) makes the host more vulnerable to further infection. Such an assumption is certainly natural for HIV, where the primary target cells are T lymphocytes.

All the simulated oscillating motions and blips presented in this paper show constant amplitudes and frequencies. This is because all parameter values are fixed in these simulations. We note, however, that nonlinear, deterministic systems can indeed generate oscillations with varying amplitudes and phases, called "amplitude modulation" and "frequency modulation" due to nonlinearity. This can be seen from (2.13), where both amplitude and phase are functions of the parameter μ. Since in reality parameters are not constant, time-varying parameters can be seen as analogous to the variation due to random perturbations in stochastic models. Although deterministic models with fixed parameter values cannot generate varying amplitude and phase, deterministic models can generate such variation if the system is nonlinear and some parameters vary with time. For example, Figure 6.1 shows the result of changing the fixed α used in Figure 2.3(c) to a time-varying deterministic function, clearly demonstrating that a deterministic model can generate blips of varying magnitude, frequency, and duration.

We note that mathematically, a system of delay differential equations (DDEs) could also generate oscillatory behaviors similar to viral blips. However, in this case, the inherent delay would need to be of the same order as the interval between blips, that is, on the order of several months. Since it is difficult to suggest a physiological or immunological process that would impose a delay of this magnitude, it seems unlikely that DDEs are the most natural approach for modeling viral blips.

While we are able to show that linear or constant infection rates do not lead

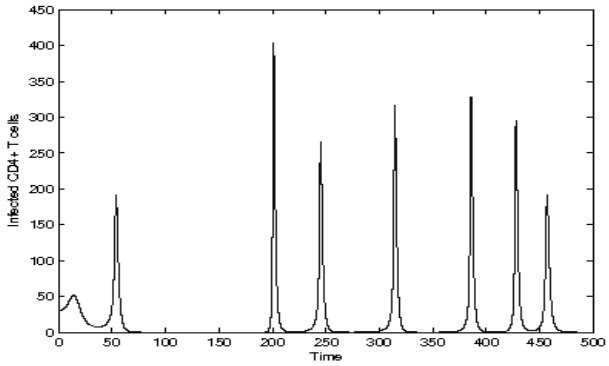

FIG. 6.1. *Simulated viral blips of system* (2.1) *with varying amplitude and frequency when using a time-varying function* $\alpha(t) = \alpha_T + \left[-0.31 + 0.3e^{-3\cos(t/50)}\cos(t/100)\right] \times 10^{13}$, *where* $\alpha_T = 4.58 \times 10^{13}$ *is the transcritical bifurcation value.*

to blips in the 2-, 3-, or 4-dimensional models we have studied, further study of a 5-dimensional immunological model reveals that a system with a constant infection rate can also generate blips. This suggests that the use of an increasing, saturating, infection rate function is not necessary but is effective in low-dimensional models. The results presented here provide a useful tool for the mathematical study of viral blips or other examples of recurrent infection. The conditions in our hypothesis may also be used or generalized to study recurrent phenomena in other physical systems.

Acknowledgments. Insightful comments from Dr. N. K. Vaidya and two referees are greatly appreciated.

REFERENCES

[1] R. M. ANDERSON AND R. M. MAY, *Population biology of infectious diseases: Part* I, Nature, 280 (1979), pp. 361–367.

[2] R. J. DE BOER AND A. S. PERELSON, *Target cell limited and immune control models of HIV infection: A comparison*, J. Theoret. Biol., 190 (1998), pp. 201–214.

[3] I. BOLDOGH, T. ALBRECHT, AND D. D. PORTER, *Persistent viral infections*, in Medical Microbiology, University of Texas Medical Branch at Galveston, Galveston, TX, 1996.

[4] B. CHAN AND P. YU, *Bifurcation analysis in a model of cytotoxic T-lymphocyte response to viral infection*, Nonlinear Anal., 13 (2012), pp. 64–77.

[5] A. C. COLLIER, R. W. COOMBS, D. A. SCHOENFELD, R. L. BASSETT, J. TIMPONE, A. BARUCH, M. JONES, K. FACEY, C. WHITACRE, V. J. MCAULIFFE, H. M. FRIEDMAN, T. C. MERIGAN, R. C. REICHMAN, C. HOOPER, AND L. COREY, *Treatment of human immunodeficiency virus infection with saquinavir, zidovudine, and zalcitabine*, New England J. Med., 334 (1996), pp. 1011–1018.

[6] J. M. CONWAY AND D. COOMBS, *A stochastic model of latently infected cell reactivation and viral blip generation in treated HIV patients*, PLoS Comput. Biol., 7 (2011), e1002033.

[7] S. DEVADAS, L. ZARITSKAYA, S. G. RHEE, L. OBERLEY, AND M. S. WILLIAMS, *Discrete generation of superoxide and hydrogen peroxide by T cell receptor stimulation: Selective regulation of mitogen-activated protein kinase activation and fas ligand expression*, J. Exper. Med., 195 (2002), pp. 59–70.

[8] G. DORNADULA, H. ZHANG, B. VANUITERT, J. STERN, L. LIVORNESE, JR., M. J. INGERMAN, J. WITEK, R. J. KEDANIS, J. NATKIN, J. DESIMONE, AND R. J. POMERANTZ, *Residual HIV-1 RNA in blood plasma of patients taking suppressive highly active antiretroviral therapy*, J. Amer. Med. Assoc., 282 (1999), pp. 1627–1632.

[9] N. M. FERGUSON, F. DE WOLF, A. C. GHANI, C. FRASER, C. A. DONNELLY, P. REISS, J. M. A. LANGE, S. A. DANNER, G. P. GARNETT, J. GOUDSMIT, AND R. M. ANDERSON, *Antigen-driven* $CD4^+$ *T cell and HIV-1 dynamics: Residual viral replication under highly active*

antiretroviral therapy, Proc. Natl. Acad. Sci. USA, 96 (1999), pp. 15167–15172.

[10] C. Fraser, N. M. Ferguson, and R. M. Anderson, *Quantification of intrinsic residual viral replication in treated HIV-infected patients*, Proc. Natl. Acad. Sci. USA, 98 (2001), pp. 15167–15172.

[11] C. Fraser, N. M. Ferguson, F. de Wolf, and R. M. Anderson, *The role of antigenic stimulation and cytotoxic T cell activity in regulating the long-term immunopathogenesis of HIV: Mechanisms and clinical implications*, Proc. Roy. Soc. B Biol. Sci., 268 (2001), pp. 2085–2095.

[12] I. C. H. Fung, M. Gambhir, A. van Sighem, F. de Wolf, and G. P. Garnett, *The clinical interpretation of viral blips in HIV patients receiving antiviral treatment: Are we ready to infer poor adherence?*, J. Acquired Immune Deficiency Syndromes, 60 (2012), pp. 5–11.

[13] M. Garland and W. W. Fawzi, *Antioxidants and progression of human immunodeficiency virus (HIV) disease*, Nutrition Res., 19 (1999), pp. 1259–1276.

[14] N. J. Garretta, V. Apeaa, A. Noria, I. Ushiro-Lumbb, A. R. Oliverb, G. Bailya, and D. A. Clarkb, *Comparison of the rate and size of HIV-*1 *viral load blips with Roche COBAS TaqMan HIV-*1 *versions* 1.0 *and* 2.0 *and implications for patient management*, J. Clinical Virol., 53 (2012), pp. 354–355.

[15] L. Gil, G. Martinez, I. Gonzalez, A. Tarinas, A. Alvarez, A. Giuliani, R. Molina, R. Tapanes, J. Perez, and O. D. Leon, *Contribution to characterization of oxidative stress in HIV/AIDS patients*, Pharm. Res., 47 (2003), pp. 217–224.

[16] G. Gloire, S. Legrand-Poels, and J. Piette, *NF-κB activation by reactive oxygen species: Fifteen years later*, Biochem. Pharm., 72 (2006), pp. 1493–1505.

[17] J. T. Grennan, M. R. Loutfy, D. Su, P. R. Harrigan, C. Cooper, M. Klein, N. Machouf, J. S. G. Montaner, S. Rourke, C. Tsoukas, B. Hogg, J. Raboud, and the CANOC Collaboration, *Magnitude of virologic blips is associated with a higher risk for virologic rebound in HIV-infected individuals: A recurrent events analysis*, J. Infectious Diseases, 205 (2012), pp. 1230–1238.

[18] S. Gropper, J. Smith, and J. Groff, *Advanced Nutrition and Human Metabolism*, 5th ed., Cengage Learning, Independence, KY, 2009.

[19] J. Guckenheimer and P. Holmes, *Nonlinear Oscillations, Dynamical Systems, and Bifurcations of Vector Fields*, Appl. Math. Sci. 42, Springer-Verlag, New York, 1983.

[20] D. A. Hildeman, *Regulation of T-cell apoptosis by reactive oxygen species*, Free Rad. Biol. Med., 36 (2004), pp. 1496–1504.

[21] D. Hinrichsen and A. J. Pritchard, *Mathematical Systems Theory* I: *Modelling, State Space Analysis, Stability and Robustness*, 2nd ed., Texts Appl. Math. 48, Springer, New York, 2005.

[22] N. Israel and M. A. Gougerot-Pocidalo, *Oxidative stress in human immunodeficiency virus infection*, Cell. Molec. Life Sciences, 53 (1997), pp. 864–870.

[23] L. E. Jones and A. S. Perelson, *Opportunistic infection as a cause of transient viremia in chronically infected HIV patients under treatment with HAART*, Bull. Math. Biol., 67 (2005), pp. 1227–1251.

[24] L. E. Jones and A. S. Perelson, *Transient viremia, plasma viral load, and reservoir replenishment in HIV infected patients on antiretroviral therapy*, J. Acquired Immune Deficiency Syndromes, 45 (2007), pp. 483–493.

[25] H. M. Lander, *An essential role for free radicals and derived species in signal transduction*, The FASEB J., 11 (1997), pp. 118–124.

[26] N. Li and M. Karin, *Is nf-κb the sensor of oxidative stress?*, The FASEB J., 13 (1999), pp. 1137–1143.

[27] M. A. Nowak and C. R. M. Bangham, *Population dynamics of immune responses to persistent viruses*, Science, 272 (1996), pp. 74–79.

[28] M. A. Nowak and R. M. May, *Virus Dynamics*, Oxford University Press, New York, 2000.

[29] G. W. Pace and C. D. Leaf, *The role of oxidative stress in HIV disease*, Free Rad. Biol. Med., 19 (1995), pp. 523–528.

[30] S. Palmer, F. Maldarelli, A. Wiegand, B. Bernstein, G. J. Hanna, S. C. Brun, D. J. Kempf, J. W. Mellors, J. M. Coffin, and M. S. King, *Low-level viremia persists for at least* 7 *years in patients on suppressive antiretroviral therapy*, Proc. Natl. Acad. Sci. USA, 105 (2008), pp. 3879–3884.

[31] S. Palmer, A. P. Wiegand, F. Maldarelli, H. Bazmi, J. M. Mican, M. Polis, R. L. Dewar, A. Planta, S. Liu, J. A. Metcalf, J. W. Mellors, and J. M. Coffin, *New real-time reverse transcriptase-initiated PCR assay with single-copy sensitivity for human immunodeficiency virus type* 1 *RNA in plasma*, J. Clinical Microbiol., 41 (2003), pp. 4531–4536.

[32] A. S. Perelson, P. Essunger, Y. Cao, M. Vesanen, A. Hurley, K. Saksela, M. Markowitz, and D. D. Ho, *Decay characteristics of HIV-1-infected compartments during combination therapy*, Nature, 387 (1997), pp. 188–191.
[33] L. Rong, Z. Feng, and A. Perelson, *Mathematical modeling of HIV-1 infection and drug therapy*, in Mathematical Modeling of Biosystems, R. P. Mondaini and P. M. Pardalos, eds., Springer-Verlag, New York, 2008, pp. 77–87.
[34] L. Rong and A. S. Perelson, *Asymmetric division of activated latently infected cells may explain the decay kinetics of the HIV-1 latent reservoir and intermittent viral blips*, Math. Biosci., 217 (2009), pp. 77–87.
[35] L. Rong and A. S. Perelson, *Modeling latently infected cell activation: Viral and latent reservoir persistence, and viral blips in HIV-infected patients on potent therapy*, PLoS Comput. Biol., 5 (2009), e1000533.
[36] K. B. Schwarz, *Oxidative stress during viral infection: A review*, Free Rad. Biol. Med., 21 (1996), pp. 641–649.
[37] C. B. Stephenson, G. S. Marquis, S. D. Douglas, and C. M. Wilson, *Immune activation and oxidative damage in HIV-positive and HIV-negative adolescents*, J. Acquired Immune Deficiency Syndromes, 38 (2005), pp. 180–190.
[38] C. B. Stephenson, G. S. Marquis, R. A. Jacob, L. A. Kruzich, S. D. Douglas, and C. M. Wilson, *Vitamins C and E in adolescents and young adults with HIV infection*, Amer. J. Clinical Nutrition, 83 (2006), pp. 870–879.
[39] R. D. van Gaalen and L. M. Wahl, *Reconciling conflicting clinical studies of antioxidant supplementation as HIV therapy: A mathematical approach*, BMC Public Health, 9 (Suppl. 1) (2009), pp. 1–18.
[40] L. P. Villarreal, V. R. Defilippis, and K. A. Gottlieb, *Acute and persistent viral life strategies and their relationship to emerging diseases*, Virology, 272 (2000), pp. 1–6.
[41] W. Yao, L. Hertel, and L. M. Wahl, *Dynamics of recurrent viral infection*, Proc. Roy. Soc. Biol. Sci., 273 (2006), pp. 2193–2199.
[42] P. Yu, *Computation of normal forms via a perturbation technique*, J. Sound Vibration, 211 (1998), pp. 19–38.
[43] P. Yu, *Closed-form conditions of bifurcation points for general differential equations*, Internat. J. Bifur. Chaos Appl. Sci. Engrg., 15 (2005), pp. 1467–1483.
[44] P. Yu and K. Huseyin, *A perturbation analysis of interactive static and dynamic bifurcations*, IEEE Trans. Automat. Control, 33 (1988), pp. 28–41.